J. Fluid Mech. (1998), *vol.* 369, *pp.* 91–123. Printed in the United Kingdom

Resonant scattering of edge waves by longshore periodic topography

By YONGZE CHEN AND R. T. GUZA

Center for Coastal Studies, Scripps Institution of Oceanography, La Jolla, CA 92093, USA

(Received 2 August 1997 and in revised form 16 March 1998)

The resonant scattering of topographically trapped, low-mode progressive edge waves by longshore periodic topography is investigated using a multiple-scale expansion of the linear shallow water equations. Coupled evolution equations for the slowly varying amplitudes of incident and scattered edge waves are derived for small-amplitude, periodic depth perturbations superposed on a plane beach. In 'single-wave scattering', an incident edge wave is resonantly scattered into a single additional progressive edge wave having the same or different mode number (i.e. longshore wavenumber), and propagating in the same or opposite direction (forward and backward scattering, respectively), as the incident edge wave. Backscattering into the same mode number as the incident edge wave, the analogue of Bragg scattering of surface waves, is a special case. In 'multi-wave scattering', simultaneous forward and backward resonant scattering results in several (rather than only one) new progressive edge waves. Analytic solutions are obtained for single-wave scattering and for a special case of multi-wave scattering involving mode-0 and mode-1 edge waves, over perturbed depth regions of both finite and semi-infinite longshore extent. In single-wave backscattering with small (subcritical) detuning (i.e. departure from exact resonance), the incident and backscattered wave amplitudes both decay exponentially with propagation distance over the periodic bathymetry, whereas with large (supercritical) detuning the amplitudes oscillate with distance. In single-wave forward scattering, the wave amplitudes are oscillatory regardless of the magnitude of the detuning. Multi-wave solutions combine aspects of single-wave backward and forward scattering. In both single- and multi-wave scattering, the exponential decay rates and oscillatory wavenumbers of the edge wave amplitudes depend on the detuning. The results suggest that naturally occurring rhythmic features such as beach cusps and crescentic bars are sometimes of large enough amplitude to scatter a significant amount of incident low-mode edge wave energy in a relatively short distance ($O(10)$ topographic wavelengths).

1. Introduction

Several recent studies concern surface water wave propagation over topography that varies periodically about a constant mean depth. A wave normally incident on a patch of periodically spaced bars on the sea floor can be strongly backscattered (i.e. reflected) if the bar wavelength is half that of the wave (i.e. Bragg reflection). The backscattered wave has the same frequency and wavenumber as the incident wave, but propagates in the opposite direction. Measured reflected wave amplitudes at resonance (Heathershaw 1982) agree well with predictions of a multiple-scale-based theory valid near and at resonance (Mei 1985). Mei (1985) stressed the role of the

critical (or 'cutoff') detuning frequency, determined by the incident wave dispersion relation and the bar geometry. Backscattering is qualitatively different when the detuning frequency (the difference between the wave frequency and the frequency for exact Bragg resonance) is above or below the critical detuning frequency. When the detuning frequency is small (subcritical), the backscatter from successive bars is strongly constructive. The amplitudes of the incident and backscattered waves both decay exponentially with propagation distance over the bars, and the incident energy is strongly reflected from the region of rhythmic bottom perturbations. On the other hand, when the detuning frequency is large (supercritical), waves backscattered from successive bars drift in and out phase. The incident and backscattered wave amplitudes oscillate over the bar region, and reflection from the undulating region is incomplete. Additional studies concern other aspects of Bragg scattering (Guazzelli, Rey & Belzons 1992; Mei & Liu 1993; Liu & Cho 1993; Rey, Guazzelli & Mei 1996; and references therein).

Fewer studies have considered the effect of rhythmic beach topography on edge wave propagation. Edge waves are longshore periodic surface gravity waves that are refractively trapped near the shoreline, where sinuous morphologies such as beach cusps and crescentic bars are sometimes well developed. Cusps and crescentic bars on ocean beaches have longshore wavelengths of O(10–50) m and O(100–500) m, respectively, comparable to those of subharmonic and infragravity edge waves, respectively. Guza & Bowen (1981) showed that beach cusps alter the dispersion relation of standing edge waves with half the cusp wavenumber, and that this alteration may have a negative feedback to the nonlinear excitation of subharmonic edge waves. However, to our knowledge there are no studies concerning the propagation of progressive edge waves over longshore periodic bathymetries, even though progressive edge waves are more commonly observed than standing edge waves (Munk, Snodgrass & Gilbert 1964; Huntley, Guza & Thornton 1981; Oltman-Shay & Guza 1987).

A theory for the resonant scattering of linear progressive low-mode edge waves by small-amplitude longshore periodic perturbations about a plane beach is developed below, using an approach similar to that used by Mei (1985) to study Bragg scattering of surface waves. In 'single-wave scattering', an incident edge wave propagating over periodic topography is resonantly scattered into a single additional progressive edge wave with the same or different mode number (i.e. longshore wavenumber), and propagating in the same or opposite direction (forward and backward scattering, respectively), as the incident edge wave. Backscattering into an edge wave with the same mode number as the incident edge wave, the analogue of Bragg scattering of surface waves in constant mean depth, is a special case of single-wave backward scattering. In 'multi-wave scattering', simultaneous forward and backward resonant scattering results in several (rather than only one) new progressive edge waves.

The paper is organized as follows. In §2 evolution equations for the amplitudes of the incident and resonantly scattered edge waves are derived for single-wave scattering and for a special case of multi-wave scattering involving mode-0 and mode-1 edge waves. General properties of the solutions are discussed in §3. In §4, results are given for scattering by periodic topographic perturbations roughly resembling observed beach cusps and crescentic sandbars. These depth perturbations are predicted to scatter significant incident progressive edge wave energy, over a considerable frequency bandwidth, within the relatively short distance of O(10) topographic wavelengths. A discussion and a summary are given in §5 and §6, respectively.

2. Evolution equations for edge wave amplitudes

Small-amplitude, low-mode edge waves are governed by the linearized shallow water equation

$$-\eta_{tt} + (gh\eta_x)_x + (gh\eta_y)_y = 0, \tag{2.1}$$

where η is the free surface displacement, h is the water depth, g is the gravitational acceleration, x and y are the offshore and longshore coordinates, and subscripted variables indicate partial derivatives. The nearshore topography is assumed planar with slope s, plus a small longshore periodic perturbation h_1 (e.g. beach cusps and crescentic bars)

$$h = h_0(x) + h_1(x, y) = sx + h_1(x, y). \tag{2.2}$$

Substitution of (2.2) into (2.1) yields

$$-\eta_{tt} + (gh_0\eta_x)_x + (gh_0\eta_y)_y = -(gh_1\eta_x)_x - (gh_1\eta_y)_y. \tag{2.3}$$

Using the period and wavelength of the incident edge wave as time and space scales, the ratio of terms on the right-hand side of (2.3) to terms on the left-hand side is $O(|\nabla h_1|/s) = \epsilon$, and it is assumed that $\epsilon \ll 1$. Although higher-order, these right-hand-side terms can cause cumulatively large scattering over many topographic wavelengths if the longshore periodicity of h_1 satisfies a resonance condition.

To consider the scattering of a mode-n edge wave propagating in the positive y-direction with (positive) wavenumber k_n and frequency ω over an undulating beach, introduce the slow variables $T = \epsilon t, Y = \epsilon y$, and the multiple-scale expansion

$$\eta = \eta_0(t, x, y, T, Y) + \epsilon\eta_1(t, x, y, T, Y) + O(\epsilon^2). \tag{2.4}$$

The slope of the unperturbed plane beach is allowed to vary slowly in the longshore direction for generality, i.e. $s = s(Y)$. Note that although the slope variation is small over a typical wavelength, it may be large over a long distance. The wavenumber k_t and cross-shore structure of the depth perturbation h_1 may also vary slowly alongshore

$$h_1 = c_0(x, Y) + \left[c_1(x, Y)\mathrm{e}^{\mathrm{i}\int^y k_t \mathrm{d}y} + *\right], \tag{2.5}$$

where $*$ denotes complex conjugate. The $c_0(x, Y)$ term corresponds to a depth profile perturbation that is not oscillatory in y.

Substituting (2.4) into (2.3) and replacing h_1 with ϵh_1 yields equations at $O(\epsilon^0)$

$$-\eta_{0tt} + (gh_0\eta_{0x})_x + gh_0\eta_{0yy} = 0, \tag{2.6}$$

and at $O(\epsilon)$

$$\begin{aligned} -\eta_{1tt} + (gh_0\eta_{1x})_x + gh_0\eta_{1yy} \\ = 2\eta_{0tT} - g\,(h_0\eta_{0Y})_y - g\left(h_0\eta_{0y}\right)_Y - (gh_1\eta_{0x})_x - (gh_1\eta_{0y})_y. \end{aligned} \tag{2.7}$$

The wavenumber of the perturbed depth k_t (2.5) is assumed to satisfy the resonance condition

$$k_t = k_n - k_m, \tag{2.8}$$

where the wavenumbers k_n and k_m of mode-n and mode-m edge waves satisfy the lowest-order edge wave dispersion relation

$$\omega^2 = gs(2n + 1)k_n = gs(2m + 1)|k_m|. \tag{2.9}$$

The shallow water assumption requires $(2N + 1)s$ small, where N is the maximum mode number considered.

2.1. *Single-wave scattering*

Anticipating that interaction between the perturbed bathymetry and the incident edge wave of mode n resonantly excites only a mode-m edge wave, write the $O(\epsilon^0)$ solution as

$$\eta_0 = \tfrac{1}{2}A_0(T, Y)\varphi_n(x, Y)\mathrm{e}^{\mathrm{i}R_n} + \tfrac{1}{2}B_0(T, Y)\varphi_m(x, Y)\mathrm{e}^{\mathrm{i}R_m} + *, \tag{2.10}$$

$$R_n = \int^y k_n(Y)\mathrm{d}y - \omega t, \quad R_m = \int^y k_m(Y)\mathrm{d}y - \omega t, \tag{2.11}$$

where R_n and R_m are the phase of mode-n and mode-m edge waves, respectively, and

$$\varphi_n(x, Y) = L_n(2k_n x)\mathrm{e}^{-k_n x}, \quad \varphi_m(x, Y) = L_m(2|k_m|x)\mathrm{e}^{-|k_m|x}, \tag{2.12}$$

with $L_j(\chi)$ the Laguerre polynomials of order j. By convention, the wavenumber k_m of the scattered edge wave is positive for forward scattering and negative for backward scattering.

The amplitudes A_0 and B_0 in (2.10), unknown functions of slow variables T and Y, are determined from solvability conditions at $O(\epsilon)$. Substituting the $O(\epsilon)$ free surface displacement η_1

$$\begin{aligned}\eta_1 = {} & \tfrac{1}{2}A_1(x, T, Y)\mathrm{e}^{\mathrm{i}R_n} + \tfrac{1}{2}B_1(x, T, Y)\mathrm{e}^{\mathrm{i}R_m} \\ & + \tfrac{1}{2}C_1(x, T, Y)\mathrm{e}^{\mathrm{i}(2R_n - R_m)} + \tfrac{1}{2}D_1(x, T, Y)\mathrm{e}^{\mathrm{i}(2R_m - R_n)} + *,\end{aligned} \tag{2.13}$$

and (2.10) into (2.7), and using the single-wave scattering assumption that only terms with phases R_n and R_m are resonant, yields equations for A_1 and B_1:

$$\begin{aligned}(\omega^2 - gh_0k_n^2)A_1 + (gh_0A_{1x})_x = {} & -2\mathrm{i}\omega\varphi_nA_{0T} - 2\mathrm{i}gh_0k_n(\varphi_nA_0)_Y \\ & - g[(c_0\varphi_{nx})_x - k_n^2c_0\varphi_n]A_0 - g[(c_1\varphi_{mx})_x - k_mk_nc_1\varphi_m]B_0,\end{aligned} \tag{2.14a}$$

and

$$\begin{aligned}(\omega^2 - gh_0k_m^2)B_1 + (gh_0B_{1x})_x = {} & -2\mathrm{i}\omega\varphi_mB_{0T} - 2\mathrm{i}gh_0k_m(\varphi_mB_0)_Y \\ & - g[(c_0\varphi_{mx})_x - k_m^2c_0\varphi_m]B_0 - g\left[(c_1^*\varphi_{nx})_x - k_nk_mc_1^*\varphi_n\right]A_0.\end{aligned} \tag{2.14b}$$

The single-wave scattering assumption implies that waves with phase $2R_n - R_m$ and $2R_m - R_n$ in (2.13) are not free, i.e. neither $(\omega, 2k_n - k_m)$ nor $(\omega, 2k_m - k_n)$ satisfies the dispersion relation (2.9) for any mode number.

Because φ_n and φ_m (2.12) are homogeneous solutions of (2.14a) and (2.14b), respectively, solvability conditions for A_1 (2.14a) and B_1 (2.14b) require

$$\int_0^{+\infty}[\text{RHS of (2.14}a\text{)}]\varphi_n\mathrm{d}x = 0, \quad \int_0^{+\infty}[\text{RHS of (2.14}b\text{)}]\varphi_m\mathrm{d}x = 0. \tag{2.15}$$

Straightforward algebra using orthogonality and recurrence relations for $L_j(\chi)$ yields

$$A_{0T} + \left(C_{gn}A_0\right)_Y = \mathrm{i}\left[\alpha_nC_{gn}A_0 + \beta_{nm}^{\pm}C_{gm}B_0\right], \tag{2.16a}$$

$$B_{0T} \pm \left(C_{gm}B_0\right)_Y = \mathrm{i}\left[\alpha_mC_{gm}B_0 + (\beta_{nm}^{\pm})^*C_{gn}A_0\right], \tag{2.16b}$$

where

$$C_{gn} = \mathrm{d}\omega/\mathrm{d}k_n = \omega/2k_n, \quad C_{gm} = \mathrm{d}\omega/\mathrm{d}|k_m| = \omega/2|k_m|, \tag{2.17}$$

are the group velocity for mode-n and mode-m edge waves, + and − signs correspond to forward and backward scattering, respectively, and

$$\alpha_j(Y) = \frac{g}{2C_{gj}^2}\int_0^{+\infty}\left[(c_0\varphi_{jx})_x - k_j^2 c_0\varphi_j\right]\varphi_j \mathrm{d}x \quad (j = n, m), \tag{2.18}$$

$$\beta_{nm}^{\pm}(Y) = \frac{g}{2C_{gm}C_{gn}}\left\{c_1|_{x=0}\frac{\omega^2}{gs} - \int_0^{+\infty} c_1\left[\varphi_{mx}\varphi_{nx} \pm |k_m|k_n\varphi_m\varphi_n\right]\mathrm{d}x\right\}. \tag{2.19}$$

The first term on the right-hand sides of (2.16*a*) and (2.16*b*) is associated with changes in the edge wave dispersion relation (2.9) owing to the perturbation c_0 of the mean (y-averaged) depth profile (see (2.18) and (2.5)). The second term on the right-hand sides couples the incident and scattered wave amplitudes (A_0 and B_0). The coupling coefficient $\beta_{nm}^{\pm}$ (2.19) has dimension of a wavenumber, and depends on the cross-shore structure c_1 of the longshore periodic depth perturbation with wavenumber k_t satisfying the resonance condition (2.8). Note that the coupling coefficient (2.19) is symmetric with respect to the incident edge wave mode number n and scattered wave mode number m, i.e. $\beta_{nm}^{\pm} = \beta_{mn}^{\pm}$. When $n = m$, β_{nn}^{-} is the coupling coefficient for the Bragg-like backscattering of mode-n edge waves.

It follows from (2.16) that

$$\left(C_{gn}|A_0|^2 + C_{gm}|B_0|^2\right)_T + \left(C_{gn}^2|A_0|^2 \pm C_{gm}^2|B_0|^2\right)_Y = 0, \tag{2.20}$$

which can be recast into

$$(E_n + E_m)_T + \left(C_{gn}E_n \pm C_{gm}E_m\right)_Y = 0, \tag{2.21}$$

where

$$E_n = \rho g|A_0|^2/4k_n, \quad E_m = \rho g|B_0|^2/4|k_m| \tag{2.22}$$

are the edge wave energies (per unit longshore length) for mode n and m. Thus, the total edge wave energy is conserved during single-wave scattering.

2.2. *Multi-wave scattering*

The single-wave scattering assumption, that the interaction of the incident and scattered waves with the topography will not excite additional free edge waves, is not always satisfied. For example, consider the case where periodic bathymetry (wavenumber $k_t = k_n - k_m = 2\omega^2/3gs$) forward scatters a mode-0 incident wave ($k_n = \omega^2/gs$) into a mode-1 wave ($k_m = \omega^2/3gs$). Note that the forward scattered mode-1 wave ($k_n = \omega^2/3gs$) is backscattered by the same bathymetry into an oppositely propagating mode-1 wave ($k_m = -\omega^2/3gs$). Thus, the forward scattering between mode-0 and mode-1, and the Bragg-like backscattering of mode 1, occur simultaneously and cannot be considered independently. The multi-wave scattering in this case eventually involves four different wave components: mode-0 and mode-1 edge waves propagating in both directions. Single-wave scattering solutions also do not apply to forward scattering of the mode pair (1, 2), nor to forward scattering of the mode pair (1, 3). With (1, 2) forward scattering the final multi-wave state involves six waves: mode 1, 2, and 7 propagating in both directions. With (1, 3) forward scattering the final state consists of three waves: mode 1 and 3 propagating in the $+y$-direction, and mode 10 in the $-y$-direction. For brevity, the only multi-wave scattering case considered here involves mode-0 and mode-1 edge waves. The analysis can readily be extended to other multi-wave scattering cases involving a high-mode edge wave, but the beach and depth perturbation slopes must then be very small for the shallow water equations to remain valid.

The $O(\epsilon^0)$ multi-wave scattering solution involving mode-0 and mode-1 edge waves is

$$\eta_0 = \tfrac{1}{2}\varphi_0(x,Y)\left[A_0^+(T,Y)\mathrm{e}^{\mathrm{i}\int^y k_0\mathrm{d}y-\mathrm{i}\omega t} + A_0^-(T,Y)\mathrm{e}^{-\mathrm{i}\int^y k_0\mathrm{d}y-\mathrm{i}\omega t}\right] + \tfrac{1}{2}\varphi_1(x,Y)\left[B_0^+(T,Y)\mathrm{e}^{\mathrm{i}\int^y k_1\mathrm{d}y-\mathrm{i}\omega t} + B_0^-(T,Y)\mathrm{e}^{-\mathrm{i}\int^y k_1\mathrm{d}y-\mathrm{i}\omega t}\right] + *, \quad (2.23)$$

with the topographic wavenumber $k_t = k_0 - k_1 = 2k_1$. Solvability conditions at $O(\epsilon)$ again yield evolution equations for the lowest-order edge wave amplitudes:

$$A_{0T}^+ + (C_{g0}A_0^+)_Y = \mathrm{i}\left[\alpha_0 C_{g0}A_0^+ + \beta_{01}^+ C_{g1}B_0^+\right], \quad (2.24a)$$

$$A_{0T}^- - (C_{g0}A_0^-)_Y = \mathrm{i}\left[\alpha_0 C_{g0}A_0^- + (\beta_{01}^+)^* C_{g1}B_0^-\right], \quad (2.24b)$$

$$B_{0T}^+ + (C_{g1}B_0^+)_Y = \mathrm{i}\left[\alpha_1 C_{g1}B_0^+ + (\beta_{01}^+)^* C_{g0}A_0^+ + \beta_{11}^- C_{g1}B_0^-\right], \quad (2.24c)$$

$$B_{0T}^- - (C_{g1}B_0^-)_Y = \mathrm{i}\left[\alpha_1 C_{g1}B_0^- + \beta_{01}^+ C_{g0}A_0^- + (\beta_{11}^-)^* C_{g1}B_0^+\right]. \quad (2.24d)$$

Note that coupling occurs between one mode-0 and one mode-1 edge wave propagating in the same direction (positive or negative y-direction) with coupling coefficient β_{01}^+, and between two mode-1 edge waves (propagating in opposite directions) with coupling coefficient β_{11}^-. No direct coupling occurs between two mode-0 edge waves (i.e. β_{00}^- does not appear in the equations). From (2.24), the total edge wave energy is again conserved,

$$\left[E_0^+ + E_0^- + E_1^+ + E_1^-\right]_T + \left[C_{g0}\left(E_0^+ - E_0^-\right) + C_{g1}\left(E_1^+ - E_1^-\right)\right]_Y = 0, \quad (2.25)$$

where

$$E_0^\pm = \rho g|A_0^\pm|^2/4k_0, \quad E_1^\pm = \rho g|B_0^\pm|^2/4k_1. \quad (2.26)$$

3. Solutions for scattered and transmitted wave fields

Assume for simplicity that the slope s of the unperturbed beach is constant (the effect of slow alongshore variation $s(Y)$ is discussed in Appendix A), and also that c_0 and c_1 in the bathymetric perturbation (2.5) are independent of the slow variable Y. The resulting constant-coefficient equations for single-wave (2.16) and multi-wave (2.24) scattering can be solved analytically. The incident edge wave with amplitude a_0 is allowed a slight frequency detuning $\epsilon\Omega$ from the resonant frequency ω and a corresponding wavenumber detuning $\epsilon\Omega/C_{gn}$ from the resonant wavenumber k_n, where Ω/ω is of order unity. Detuned solutions are used in §4 to determine the frequency range of incident edge waves that are strongly scattered by periodic beach cusps and crescentic bars.

3.1. *Single-wave backward scattering*

3.1.1. *Over a finite region*

Edge waves backscattered by a finite-length longshore topographic perturbation spanning $0 \leqslant Y \leqslant L$ must have zero amplitude on the transmitted side, i.e.

$$B_0 = 0, \quad Y \geqslant L. \quad (3.1)$$

Over the undulating region, the scattered and transmitted wave amplitudes are governed by (2.16) with − sign. With

$$A_0 = a_0 T(Y) \mathrm{e}^{\mathrm{i}[(\alpha_n - \alpha_m + \Omega/C_{gn} - \Omega/C_{gm})Y/2 - \Omega T]}, \quad 0 \leqslant Y \leqslant L, \tag{3.2a}$$

$$B_0 = a_0 (C_{gn}/C_{gm}) S(Y) \mathrm{e}^{\mathrm{i}[(\alpha_n - \alpha_m + \Omega/C_{gn} - \Omega/C_{gm})Y/2 - \Omega T]}, \quad 0 \leqslant Y \leqslant L, \tag{3.2b}$$

the wave fields on the incident ($Y \leqslant 0$) and transmitted sides ($Y \geqslant L$) of the undulating region are

$$A_0 = a_0 \mathrm{e}^{\mathrm{i}\Omega(Y/C_{gn} - T)}, \quad B_0 = a_0 (C_{gn}/C_{gm}) S(0) \mathrm{e}^{\mathrm{i}\Omega(-Y/C_{gm} - T)}, \quad Y \leqslant 0, \tag{3.3}$$

and

$$A_0 = a_0 T(L) \mathrm{e}^{\mathrm{i}(\alpha_n - \alpha_m + \Omega/C_{gn} - \Omega/C_{gm})L/2} \mathrm{e}^{\mathrm{i}\Omega[(Y-L)/C_{gn} - T]}, \quad B_0 = 0, \quad Y \geqslant L. \tag{3.4}$$

Continuity conditions for A_0 and B_0 at $Y = 0$ and $Y = L$ are satisfied if $T(0) = 1$ and $S(L) = 0$, respectively. The solutions for $T(Y)$ and $S(Y)$ are exponential or oscillatory, depending on whether the magnitude of the total effective detuning wavenumber

$$K = \left(\alpha_n + \alpha_m + \Omega/C_{gn} + \Omega/C_{gm}\right)/2 \tag{3.5}$$

is less or greater than the coupling coefficient $|\beta_{nm}^-|$ (2.19). The coupling coefficient $|\beta_{nm}^-|$ is thus the critical (or cutoff) detuning wavenumber. Note that the total effective detuning wavenumber K is the sum of the averaged (over the incident and scattered waves) detuning corresponding to the frequency detuning in the incident wave Ω and the averaged detuning caused by small changes in the dispersion relation associated with perturbation of the mean (y-averaged) bathymetry (the α terms in (3.5) depend on c_0, see (2.18) and (2.5)).

The squared scattering and transmission coefficients, defined as the ratio of the scattered and incident wave energy fluxes to the incident wave flux at the upwave edge of the perturbed region $Y = 0$, respectively, are $|S(Y)|^2$ and $|T(Y)|^2$ according to (3.2*a*) and (3.2*b*). Energy conservation (from (2.20)) yields

$$|T(Y)|^2 - |S(Y)|^2 = 1 - |S(0)|^2 > 0. \tag{3.6}$$

Maxima of the scattered and transmitted wave amplitudes therefore occur at the same Y location (so do the minima), and $|T(L)|^2 + |S(0)|^2 = 1$.

Case (i): $K^2 < |\beta_{nm}^-|^2$ (subcritical detuning)

When the magnitude of the effective detuning wavenumber is below cutoff, solutions for $T(Y)$ and $S(Y)$ ((3.2*a*) and (3.2*b*)) over the undulating region $0 \leqslant Y \leqslant L$ are

$$T(Y) = \frac{Q \cosh Q(L-Y) - \mathrm{i}K \sinh Q(L-Y)}{Q \cosh QL - \mathrm{i}K \sinh QL}, \tag{3.7a}$$

$$S(Y) = \frac{\mathrm{i}(\beta_{nm}^-)^* \sinh Q(L-Y)}{Q \cosh QL - \mathrm{i}K \sinh QL}, \tag{3.7b}$$

where

$$Q = \left[|\beta_{nm}^-|^2 - K^2\right]^{1/2} > 0. \tag{3.8}$$

The squared scattering coefficient over the corrugated region

$$|S(Y)|^2 = \frac{\sinh^2\left[|\beta_{nm}^-| L \left(1 - K^2/|\beta_{nm}^-|^2\right)^{1/2} (1 - Y/L)\right]}{\cosh^2\left[|\beta_{nm}^-| L \left(1 - K^2/|\beta_{nm}^-|^2\right)^{1/2}\right] - K^2/|\beta_{nm}^-|^2}, \tag{3.9}$$

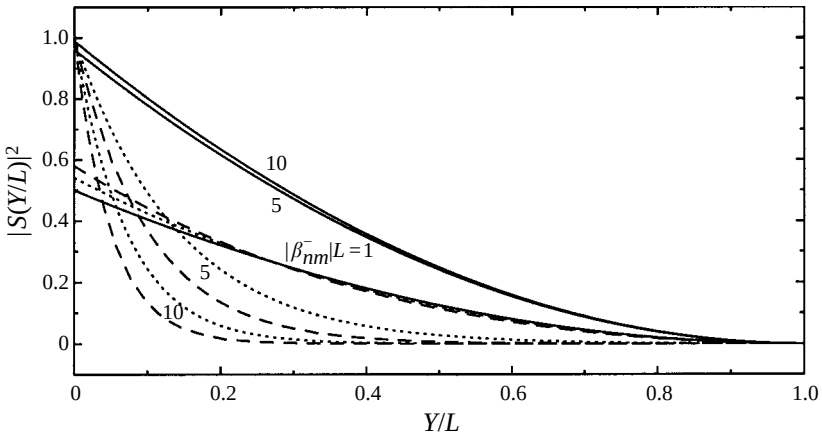

FIGURE 1. Spatial variation of the squared backward scattering coefficient $|S|^2$ over the undulating region for different region lengths $|\beta_{nm}^-|L = 1$, 5, and 10 (as indicated in the figure), when the magnitude of the effective detuning wavenumber is below or at cutoff $|\beta_{nm}^-|$: - - -, $K^2/|\beta_{nm}^-|^2 = 0$; $\cdots$, $K^2/|\beta_{nm}^-|^2 = 0.5$; ——, $K^2/|\beta_{nm}^-|^2 = 1$.

depends on both $K^2/|\beta_{nm}^-|^2$ and $|\beta_{nm}^-|L$, the normalized detuning wavenumber and the normalized length of the undulating region, respectively. $|S(Y)|^2$ is maximum at $Y = 0$ and decays exponentially with increasing Y (see broken lines in figure 1). The transmission coefficient $|T(Y)|^2$ also decays exponentially over the undulating region (see (3.6)). Backscattering from the perturbed region is nearly complete (i.e. $|S(0)| \approx 1$) if the undulating region is sufficiently long. When $K = 0$ (perfect tuning), backscatter (i.e. $|S(0)|$) is maximized for a given $|\beta_{nm}^-|L$ (figures 1 and 3), and (3.7) reduces to

$$T(Y) = \frac{\cosh|\beta_{nm}^-|(L-Y)}{\cosh|\beta_{nm}^-|L}, \quad S(Y) = \frac{\mathrm{i}(\beta_{nm}^-)^* \sinh|\beta_{nm}^-|(L-Y)}{|\beta_{nm}^-|\cosh|\beta_{nm}^-|L}. \tag{3.10}$$

Case (ii): $K^2 = |\beta_{nm}^-|^2$ (critical detuning)

When the magnitude of the effective detuning wavenumber equals the cutoff,

$$T(Y) = \frac{1-\mathrm{i}K(L-Y)}{1-\mathrm{i}KL}, \quad S(Y) = \frac{\mathrm{i}(\beta_{nm}^-)^*(L-Y)}{1-\mathrm{i}KL}, \tag{3.11}$$

for $0 \leqslant Y \leqslant L$. The squared scattering coefficient

$$|S(Y)|^2 = (|\beta_{nm}^-|L)^2(1-Y/L)^2/[1+(|\beta_{nm}^-|L)^2], \tag{3.12}$$

monotonically decreases from $(|\beta_{nm}^-|L)^2/\left[1+(|\beta_{nm}^-|L)^2\right]$ to 0 as Y increases from 0 to L (see solid lines in figure 1).

Case (iii): $K^2 > |\beta_{nm}^-|^2$ (supercritical detuning)

When the effective detuning wavenumber magnitude is above cutoff,

$$T(Y) = \frac{P\cos P(L-Y) - \mathrm{i}K\sin P(L-Y)}{P\cos PL - \mathrm{i}K\sin PL}, \tag{3.13a}$$

$$S(Y) = \frac{\mathrm{i}(\beta_{nm}^-)^*\sin P(L-Y)}{P\cos PL - \mathrm{i}K\sin PL}, \tag{3.13b}$$

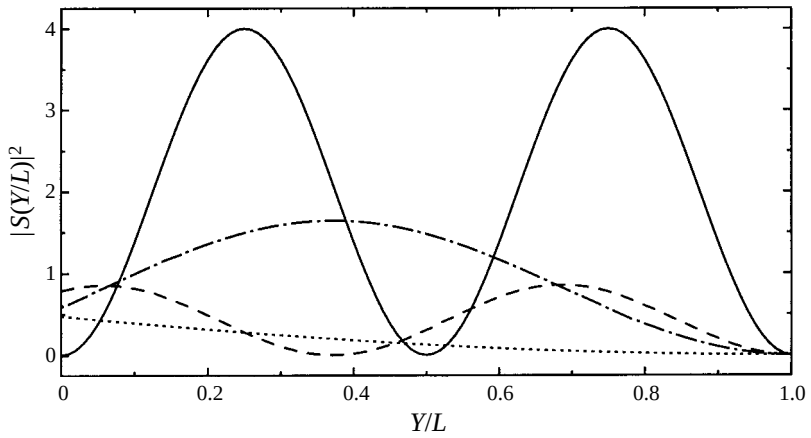

FIGURE 2. Spatial variation of $|S|^2$ over the undulating region when the magnitude of the effective detuning wavenumber is above cutoff (here $K^2/|\beta_{nm}^-|^2 = 1.25$) for different region lengths $|\beta_{nm}^-|L$: $\cdots$, 1; $-\cdot-$, 5; - - -, 10; ——, 4π.

for $0 \leqslant Y \leqslant L$, where

$$P = \left[K^2 - |\beta_{nm}^-|^2\right]^{1/2} > 0. \tag{3.14}$$

The scattering and transmission coefficients $|S(Y)|$ and $|T(Y)|$ are oscillatory over $0 \leqslant Y \leqslant L$, and

$$|S(Y)|^2 = \frac{\sin^2\left[|\beta_{nm}^-|L\left(K^2/|\beta_{nm}^-|^2 - 1\right)^{1/2}(1 - Y/L)\right]}{K^2/|\beta_{nm}^-|^2 - \cos^2\left[|\beta_{nm}^-|L\left(K^2/|\beta_{nm}^-|^2 - 1\right)^{1/2}\right]} \tag{3.15}$$

depends on the detuning $K^2/|\beta_{nm}^-|^2$ and the length of the perturbed region $|\beta_{nm}^-|L$, as in the subcritical detuning case. The spatial variation of the squared scattering coefficient over the undulating region for different values of $|\beta_{nm}^-|L$ with fixed $K^2/|\beta_{nm}^-|^2 = 1.25$ is shown in figure 2. The maximum backscattering coefficient at $Y = 0$, $\max_{|\beta_{nm}^-|L>0}\{|S(0)|\} = |\beta_{nm}^-|/K$, achieved when $|\beta_{nm}^-|L = (l - 1/2)\pi\left(K^2/|\beta_{nm}^-|^2 - 1\right)^{-1/2}$ $(l = 1, 2, \ldots)$, is always less than 1.

However, the scattering coefficient can exceed 1 inside the undulating region (figure 2). For a given $K^2/|\beta_{nm}^-|^2$, when

$$|\beta_{nm}^-|L = l\pi\left(K^2/|\beta_{nm}^-|^2 - 1\right)^{-1/2}, \quad l = 1, 2, \ldots, \tag{3.16}$$

and at locations $Y_j/L = 1 - (j - 1/2)/l$ $(j = 1, 2, \ldots, l)$, the denominator of (3.15) reaches its minimum $(K^2/|\beta_{nm}^-|^2 - 1)$, while the numerator reaches its maximum 1. The scattering coefficient at these locations

$$|S(Y_j)| = \left(K^2/|\beta_{nm}^-|^2 - 1\right)^{-1/2}, \tag{3.17}$$

is the maximum scattering coefficient (for a fixed $K^2/|\beta_{nm}^-|^2$) over the entire undulating region for any length L (the solid line in figure 2 corresponds to $l = 2$ in (3.16)). The maximum scattering coefficient (3.17) exceeds 1 when $1 < K^2/|\beta_{nm}^-|^2 < 2$, and is unbounded as $K^2/|\beta_{nm}^-|^2 \to 1$ (the length of the corrugated region L (3.16) also is unbounded in this limit). Note that condition (3.16) implies $|S(0)| = 0$ (i.e. perfect transmission), and consequently $|T(Y)|^2 = 1 + |S(Y)|^2$ according to (3.6). When the maximum squared scattering coefficient exceeds 1, the corresponding squared

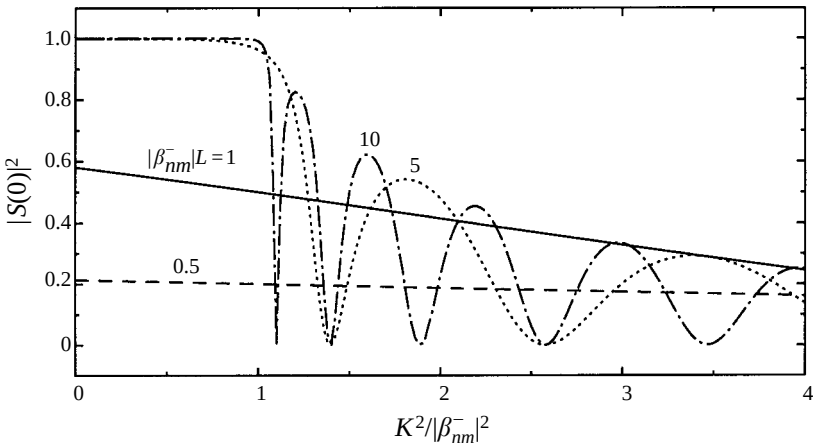

FIGURE 3. Squared backward scattering coefficient at the upwave end of the perturbed region $|S(0)|^2$ versus the detuning $K^2/|\beta_{nm}^-|^2$, for the different fixed lengths of the undulating region $|\beta_{nm}^-|L$ indicated in the figure.

transmission coefficient at the same location exceeds 2, i.e. $|T(Y_j)|^2 > 2$. Therefore, when the normalized effective detuning wavenumber $K^2/|\beta_{nm}^-|^2$ is supercritical but less than 2, the scattered and transmitted wave amplitudes are both amplified at some locations over an undulating region that allows perfect transmission (i.e. (3.16) is satisfied). Similar amplification over the bars occurs in the solutions for supercritical Bragg scattering of surface waves in constant depth, but was not mentioned by Mei (1985).

Differences between subcritical and supercritical backscattering are illustrated by the variation of $|S(0)|^2$ as a function of the detuning $K^2/|\beta_{nm}^-|^2$ (figure 3). Below and at cutoff ($K^2/|\beta_{nm}^-|^2 \leqslant 1$), $|S(0)|^2$ rises to unity rapidly and monotonically as the length of the perturbed region $|\beta_{nm}^-|L$ increases, implying nearly complete backscatter unless the undulating region is relatively short (e.g. $|\beta_{nm}^-|L \leqslant 1$). Above cutoff, backscatter is never complete and (at fixed $|\beta_{nm}^-|L$) $|S(0)|^2$ oscillates and attenuates with increasing detuning $K^2/|\beta_{nm}^-|^2$. The change in the amplitude variation over the undulating region from exponential (figure 1) to oscillatory (figure 2) that occurs at the cutoff detuning (i.e. $K^2 = |\beta_{nm}^-|^2$) is thus accompanied by a reduction in the energy backscattered from the entire undulating region (figure 3).

3.1.2. *Over a semi-infinite region*

For subcritical detuning ($K^2 < |\beta_{nm}^-|^2$), the solution (3.7) for finite undulating regions can be extended to a semi-infinite region by letting $L \to \infty$, yielding

$$T(Y) = \mathrm{e}^{-QY}, \quad S(Y) = \mathrm{i}(\beta_{nm}^-)^* \mathrm{e}^{-QY}/(Q - \mathrm{i}K), \quad 0 \leqslant Y < +\infty. \tag{3.18}$$

The scattering over the semi-infinite undulating region is complete (i.e. $|S(0)| = 1$), and the penetration distance (i.e. e-folding distance) of both the incident and backscattered edge waves into the undulating region is

$$Q^{-1} = \left[|\beta_{nm}^-| \left(1 - K^2/|\beta_{nm}^-|^2\right)^{1/2}\right]^{-1}. \tag{3.19}$$

Note that $Q^{-1} \geqslant 1/|\beta_{nm}^-|$ and increases as $K^2/|\beta_{nm}^-|^2$ increases. For Bragg scattering (i.e. $n = m$), the incident and scattered edge waves form a standing edge wave with amplitude that decays exponentially with increasing distance (Y) over the corrugated

region

$$\eta_0 = 2a_0 e^{-QY} \varphi_n(x) \cos(\omega t + \Omega T + \phi/2) \cos(k_n y + \phi/2), \tag{3.20}$$

where

$$\phi = \theta - \pi/2 - \arcsin(K/|\beta_{nn}^-|), \tag{3.21}$$

and θ is the phase in the periodic depth perturbation

$$h_1 = c_0(x) + 2c_1(x) \cos(2k_n y + \theta), \tag{3.22}$$

with c_1 real. The phase difference between the standing edge wave (3.20) and the periodic perturbed depth (3.22) is

$$\phi - \theta = -\pi/2 - \arcsin(K/|\beta_{nn}^-|). \tag{3.23}$$

For perfect tuning ($K = 0$), the phase difference ($-\pi/2$) indicates that standing wave nodes and antinodes occur at midpoints between adjacent extrema of the perturbed depth h_1.

For supercritical detuning ($K^2 > |\beta_{nm}^-|^2$), the radiation condition that the backscattered wave amplitude vanishes at $Y = +\infty$ cannot be satisfied, and there are no solutions wherein the backward travelling wave arises solely from scattering of the incident wave. Instead, the general solutions over the semi-infinite undulating region

$$T(Y) = C_1 e^{iPY} + C_2 e^{-iPY}, \tag{3.24a}$$

$$S(Y) = -C_1(\beta_{nm}^-)^* e^{iPY}/(P + K) + C_2(\beta_{nm}^-)^* e^{-iPY}/(P - K), \tag{3.24b}$$

correspond to wave energy sources at $Y = \pm\infty$, and in general the amplitudes and phases of both the incident and backward travelling waves vary periodically. There are special cases (e.g. $C_1 = 1$ and $C_2 = 0$) where the phases of these two counter-propagating waves vary over the corrugated region, but their amplitudes ($|T(Y)|$ and $|S(Y)|$) remain constant.

For critical detuning ($K^2 = |\beta_{nm}^-|^2$),

$$T(Y) = 1, \quad S(Y) = -(\beta_{nm}^-)^*/K, \quad 0 \leqslant Y < +\infty, \tag{3.25}$$

which also can be found by letting $L \to \infty$ in (3.11). The amplitudes and phases of the incoming and backward travelling waves are constant over the corrugated region. The undulating bathymetry has no effect, other than to determine the phase differences between the waves and the perturbed depth. When $n = m$, the incident and backward travelling waves form a standing wave with phase difference relative to the perturbed depth (3.22) of either π or 0, depending on whether the detuning K is positive or negative. The standing edge wave nodes and antinodes thus occur at the extrema of the depth perturbation.

Guza & Bowen (1981) showed that beach cusps with infinite extent can alter the dispersion relation of standing edge waves with twice the cusp length. Their solution for mode 0 is extended to mode n in Appendix B, and additional solutions for two counter-propagating edge waves with the same mode number over an infinite corrugated region are given.

3.2. *Single-wave forward scattering*

Single-wave forward scattering is mathematically simpler than backscattering because (2.16) becomes an initial-value problem (in space) and admits only oscillatory solutions irrespective of the magnitude of the detuning. Forward scattering from a finite-length undulating region is easily obtained from the results for a semi-infinite region so a semi-infinite region is considered first.

3.2.1. *Over a semi-infinite region*

The forward scattered edge wave must have zero amplitude over the unperturbed bathymetry

$$B_0 = 0, \quad Y \leqslant 0. \tag{3.26}$$

Solutions for A_0 and B_0 over the undulating region $Y \geqslant 0$, governed by (2.16) with + sign and satisfying the continuity boundary conditions at $Y = 0$, are

$$A_0 = a_0 T(Y) e^{i[(\alpha_n+\alpha_m+\Omega/C_{gn}+\Omega/C_{gm})Y/2-\Omega T]}, \quad Y \geqslant 0, \tag{3.27a}$$

$$B_0 = a_0 (C_{gn}/C_{gm}) S(Y) e^{i[(\alpha_n+\alpha_m+\Omega/C_{gn}+\Omega/C_{gm})Y/2-\Omega T]}, \quad Y \geqslant 0, \tag{3.27b}$$

where

$$T(Y) = \cos PY + iKP^{-1} \sin PY, \quad S(Y) = i(\beta^+_{nm})^* P^{-1} \sin PY, \tag{3.28}$$

$$P = \left[K^2 + |\beta^+_{nm}|^2\right]^{1/2} \tag{3.29}$$

(compare (3.29) with (3.14)), and K is the effective detuning wavenumber defined as

$$K = \left(\alpha_n - \alpha_m + \Omega/C_{gn} - \Omega/C_{gm}\right)/2 \tag{3.30}$$

(compare (3.30) with (3.5)). The squared scattering and transmission coefficients, $|S(Y)|^2$ and $|T(Y)|^2$, vary periodically in Y with wavenumber $2P$ and satisfy energy conservation (from (2.20) with + sign)

$$|T(Y)|^2 + |S(Y)|^2 = 1. \tag{3.31}$$

In contrast to backward scattering, when the forward scattered wave amplitude is maximum, the transmitted wave amplitude at the same location is minimum, and vice versa (contrast (3.31) with (3.6)). The squared forward scattering coefficient is

$$|S(Y)|^2 = \sin^2 PY / [K^2/|\beta^+_{nm}|^2 + 1]. \tag{3.32}$$

With perfect tuning ($K = 0$), the energy exchange between mode n and m is complete (i.e. $|S(Y)|^2 = 1$) when $|\beta^+_{nm}|Y = \pi/2, 3\pi/2$, etc. As the detuning $K^2/|\beta^+_{nm}|^2$ increases, the wavelength and maximum value of $|S(Y)|^2$ gradually decrease (energy exchange is partial).

3.2.2. *Over a finite region*

When the region of longshore undulations has finite length L, wave amplitudes are spatially uniform downwave of the depth perturbation ($Y \geqslant L$). In the undulating region $0 \leqslant Y \leqslant L$, $S(Y)$ and $T(Y)$ are still given by (3.28) so the forward scattering coefficient of the entire region $|S(L)|$ is given by (3.32) with $Y = L$ (figure 4). At exact resonance $K = 0$, forward scattering is complete ($|S(L)| = 1$) when $|\beta^+_{nm}|L = (l-1/2)\pi (l = 1, 2, \ldots)$, and transmission is complete ($|S(L)| = 0$) when $|\beta^+_{nm}|L = l\pi$. For non-zero detuning ($K \neq 0$), transmission is perfect when $PL = l\pi$, corresponding to $|\beta^+_{nm}|L = l\pi \left[K^2/|\beta^+_{nm}|^2 + 1\right]^{-1/2}$, but forward scattering is never complete (i.e. $|S(L)| < 1$ for $K \neq 0$). The values of the local maxima of the squared forward scattering coefficient $|S(L)|^2$, i.e. $\left[K^2/|\beta^+_{nm}|^2 + 1\right]^{-1}$ from (3.32), decrease as the detuning $K^2/|\beta^+_{nm}|^2$ increases, similar to the decrease in the local maxima of the squared supercritical backscattering coefficient $|S(0)|^2$ with increasing detuning (compare figures 3 with 4 for $K^2/|\beta^+_{nm}|^2 > 1$).

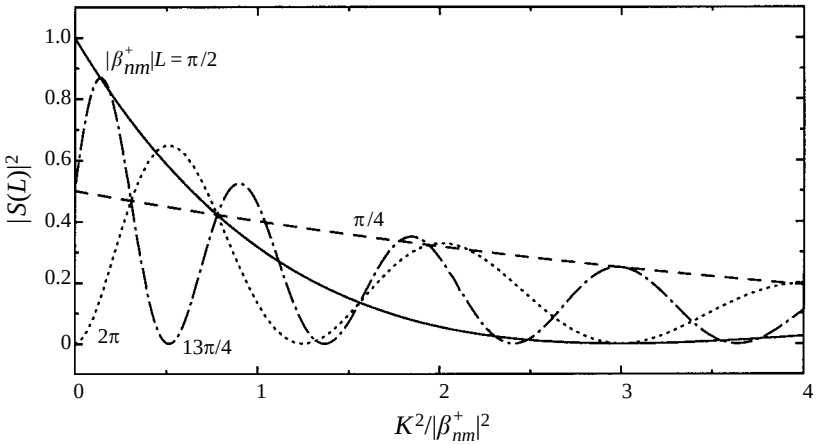

FIGURE 4. Squared forward scattering coefficient at the downwave end of the perturbed region $|S(L)|^2$ versus the detuning $K^2/|\beta^+_{nm}|^2$, for the different fixed lengths of the undulating region $|\beta^+_{nm}|L$ indicated in the figure.

3.3. *Multi-wave scattering*

To find the analytic solutions for the multi-wave scattering involving mode-0 and mode-1 edge waves, we further assume that the mean (y-averaged) profile does not deviate from the plane beach, i.e. $c_0 = 0$.

3.3.1. *Over a finite region*

The general solutions of the constant-coefficient equations (2.24) over the undulating region $0 \leqslant Y \leqslant L$ depend on the roots of the eigen equation

$$\left[\sigma^2 - (\bar{\sigma}^2 + \Delta^{1/2})/2\right]\left[\sigma^2 - (\bar{\sigma}^2 - \Delta^{1/2})/2\right] = 0, \tag{3.33a}$$

where

$$\bar{\sigma}^2 = \tilde{\alpha}_0^2 + \tilde{\alpha}_1^2 + 2|\beta^+_{01}|^2 - |\beta^-_{11}|^2, \tag{3.33b}$$

$$\Delta = \left[\tilde{\alpha}_0^2 - \tilde{\alpha}_1^2 + |\beta^-_{11}|^2\right]^2 + 4|\beta^+_{01}|^2\left[(\tilde{\alpha}_0 + \tilde{\alpha}_1)^2 - |\beta^-_{11}|^2\right], \tag{3.33c}$$

and

$$\tilde{\alpha}_0 = \Omega/C_{g0} = 2k_0\Omega/\omega, \qquad \tilde{\alpha}_1 = \Omega/C_{g1} = 2k_0\Omega/3\omega, \tag{3.33d,e}$$

which in turn depend on the frequency detuning of the incident wave Ω.

When

$$\Omega^2 = \Omega_1^2 = \frac{9\omega^2}{32k_0^2}\left[-(4|\beta^+_{01}|^2 + |\beta^-_{11}|^2) + 2|\beta^+_{01}|\left(4|\beta^+_{01}|^2 + 3|\beta^-_{11}|^2\right)^{1/2}\right], \tag{3.34}$$

$\Delta = 0$, and the eigen equation (3.33) has roots $\pm\sigma_1 = \pm\bar{\sigma}/2^{1/2}$ with double multiplicity. The corresponding general solution for (2.24) can be written as

$$\{A_0^+, A_0^-, B_0^+, B_0^-\}^{\mathrm{T}} = \mathbf{C}_1\{\mathrm{e}^{\mathrm{i}\sigma_1 Y}, Y\,\mathrm{e}^{\mathrm{i}\sigma_1 Y}, \mathrm{e}^{-\mathrm{i}\sigma_1 Y}, Y\,\mathrm{e}^{-\mathrm{i}\sigma_1 Y}\}^{\mathrm{T}}\mathrm{e}^{-\mathrm{i}\Omega T}, \tag{3.35}$$

where $\mathbf{C}_1$ is a 4×4 matrix and superscript T denotes matrix transpose. On the other hand, when

$$\Omega^2 = \Omega_2^2 = \frac{3\omega^2}{8k_0^2}\left[2|\beta_{01}^+|^2 + 3|\beta_{11}^-|^2 - |\beta_{11}^-|\left(12|\beta_{01}^+|^2 + 9|\beta_{11}^-|^2\right)^{1/2}\right], \tag{3.36}$$

or

$$\Omega^2 = \Omega_3^2 = \frac{3\omega^2}{8k_0^2}\left[2|\beta_{01}^+|^2 + 3|\beta_{11}^-|^2 + |\beta_{11}^-|\left(12|\beta_{01}^+|^2 + 9|\beta_{11}^-|^2\right)^{1/2}\right], \tag{3.37}$$

(3.33) has roots $\pm\bar{\sigma}$ and 0 with double multiplicity. The corresponding general solution for (2.24) can be expressed as

$$\{A_0^+, A_0^-, B_0^+, B_0^-\}^{\mathrm{T}} = \mathbf{C}_2\{\mathrm{e}^{\mathrm{i}\bar{\sigma}Y}, \mathrm{e}^{-\mathrm{i}\bar{\sigma}Y}, 1, Y\}^{\mathrm{T}}\mathrm{e}^{-\mathrm{i}\Omega T}, \tag{3.38}$$

where $\mathbf{C}_2$ is a 4×4 matrix.

When the frequency detuning Ω^2 does not equal Ω_1^2, Ω_2^2, or Ω_3^2, (3.33) has four distinct roots $\pm\sigma_+$ and $\pm\sigma_-$, where

$$\sigma_\pm^2 = (\bar{\sigma}^2 \pm \Delta^{1/2})/2, \tag{3.39}$$

and the general solution for (2.24) is given by

$$\{A_0^+, A_0^-, B_0^+, B_0^-\}^{\mathrm{T}} = \mathbf{C}_3\{\mathrm{e}^{\mathrm{i}\sigma_+ Y}, \mathrm{e}^{-\mathrm{i}\sigma_+ Y}, \mathrm{e}^{\mathrm{i}\sigma_- Y}, \mathrm{e}^{-\mathrm{i}\sigma_- Y}\}^{\mathrm{T}}\mathrm{e}^{-\mathrm{i}\Omega T}, \tag{3.40}$$

where $\mathbf{C}_3$ is a 4×4 matrix. For brevity, the lengthy expressions for the elements of $\mathbf{C}_j (j = 1, 2, 3)$ are not given.

For the beach cusps and crescentic bar discussed in the next section, $|\Omega_1| < |\Omega_2| < |\Omega_3|$. When $0 \leqslant |\Omega| < |\Omega_1|$, σ_+ and σ_- are complex conjugates because $\Delta < 0$. When $|\Omega| > |\Omega_1|$, σ_+ becomes real and increases with increasing $|\Omega|$, whereas σ_- is real only when $|\Omega_1| < |\Omega| < |\Omega_2|$ and $|\Omega| > |\Omega_3|$. Otherwise (i.e. when $|\Omega_2| < |\Omega| < |\Omega_3|$) σ_- is pure imaginary.

For simplicity, consider a mode-0 or mode-1 incident edge wave propagating over beach cusps with longshore wavelength $\lambda_c = 3\pi/k_0$ and a λ_c-scaled exponential cross-shore decay. The bathymetric perturbation $\epsilon h_1(x, y) = a_c \mathrm{e}^{-\pi x/\lambda_c}\cos(2\pi y/\lambda_c)$, where a_c is the cusp amplitude, is a special case of a more general cusp perturbation discussed in §4 (corresponding to $p = 1/3$ and $q = 0$ in (4.1)). The solutions over this particular topographic perturbation depend on the incident wave. Results for an incident mode-0 edge wave are presented first, followed by results for a mode-1 incident wave. The ratio of mode-n edge wave energy flux to the incident wave flux at the upwave edge of the perturbed region ($Y = 0$) is denoted as $|F_n(Y)|^2$ if the wave is forward propagating or $|B_n(Y)|^2$ if the wave is backward propagating. The variations of energy fluxes over cusped regions of different lengths for a perfectly tuned mode-0 incident wave are shown in figure 5. When $|\beta_{01}^+\beta_{11}^-|^{1/2}L = 1$ (figure 5*a*), the corrugated region is long enough such that most of the mode-0 incident edge wave energy is forward scattered to mode-1, but not long enough for significant backscattering of the mode-1 wave (note that $|\beta_{01}^+| \approx 2.7|\beta_{11}^-|$). Backscattering is insignificant in this case of a mode-0 incident wave over a moderately short scattering region, and the multi-wave equations (2.24) can be approximated by single-wave forward scattering equations (2.16). However, as the region length increases the fluxes of all the wave components vary (figures 5*b*–5*d*). The maximum energy flux of the forward propagating mode 1 ($|F_1(Y/L)|^2$) decreases, whereas the maximum fluxes of the backward propagating modes ($|B_0(Y/L)|^2$ and $|B_1(Y/L)|^2$) increase.

For a sufficiently long perturbed region, no energy reaches the downwave end of the perturbed bathymetry (figure 5*d*). Over the perturbed bathymetry, the two mode-0

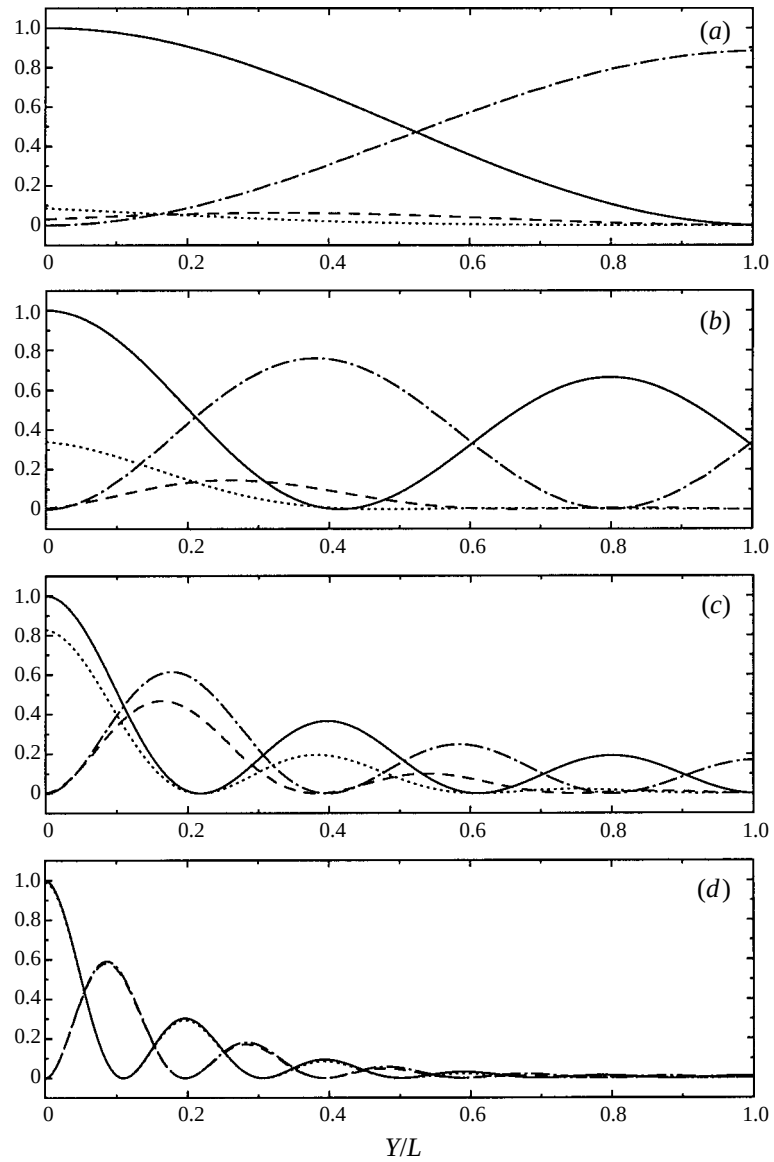

FIGURE 5. Spatial variations of energy fluxes (——, $|F_0(Y/L)|^2$; — · —, $|F_1(Y/L)|^2$; · · · ·, $|B_0(Y/L)|^2$; and - - -, $|B_1(Y/L)|^2$) of multi-wave solutions over cusped regions of different lengths: $|\beta_{01}^{+}\beta_{11}^{-}|^{1/2}L = 1.0$ (*a*), 2.5 (*b*), 5.0 (*c*), and 10.0 (*d*). The tuning is perfect ($\Omega = 0$) and the incident wave is mode 0.

edge waves have similar amplitudes and approximately form a standing edge wave, as do the two mode-1 edge waves. Upwave of the periodic bathymetry ($Y \leqslant 0$), the mode-1 energy flux is very small. Thus, to an upwave observer the effect on an incident mode-0 edge wave (with wavenumber k_0) of multi-wave scattering over a long region of periodic bathymetry with wavenumber $2k_0/3$ is nearly complete backscattering of the incident wave into a wave with the same wavenumber. Except for a possible phase difference, this is the same effect as Bragg scattering of the mode-0 incident wave by an undulating region with wavenumber $2k_0$.

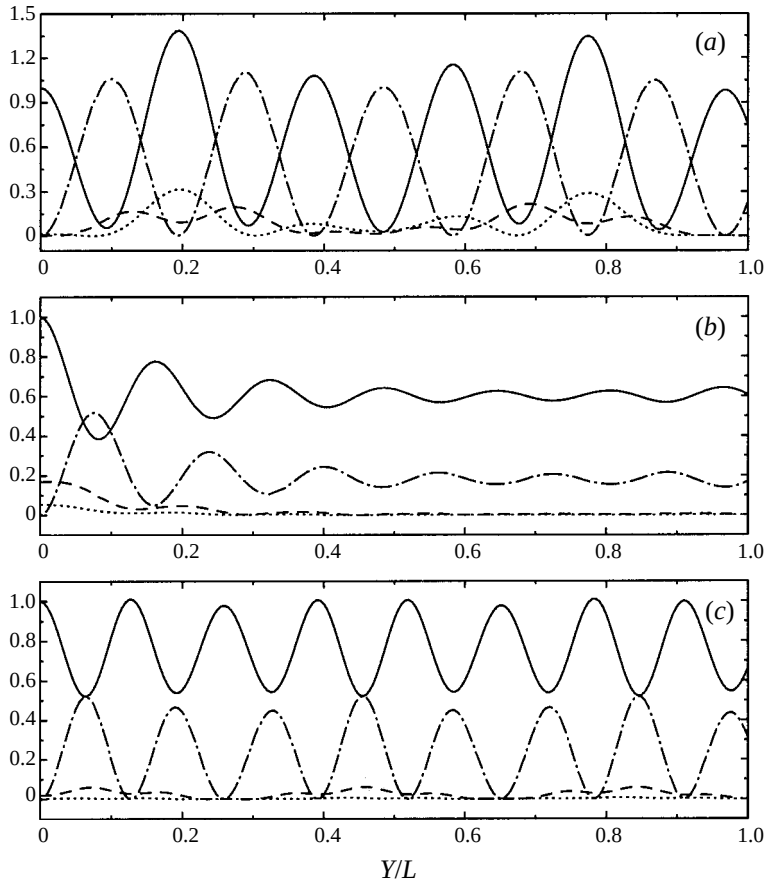

FIGURE 6. Spatial variations of energy fluxes (——, $|F_0(Y/L)|^2$; $-\cdot-$, $|F_1(Y/L)|^2$; $\cdots$, $|B_0(Y/L)|^2$; and - - -, $|B_1(Y/L)|^2$) of multi-wave solutions over beach cusps spanning a fixed length $|\beta_{01}^+\beta_{11}^-|^{1/2}L = 10.0$, for different detuning $k_0|\beta_{01}^+\beta_{11}^-|^{-1/2}|\Omega|/\omega = 0.5$ (*a*), 1.5 (*b*), and 2.5 (*c*). Zero detuning is shown in figure 5(*d*).

Frequency detuning $|\Omega|$ has a strong effect on variations of the normalized energy fluxes over a long beach cusp region, as shown in figure 6 for the detuning regions $|\Omega_1| < |\Omega| < |\Omega_2|$, $|\Omega_2| < |\Omega| < |\Omega_3|$, and $|\Omega| > |\Omega_3|$ (note that for the particular beach cusps considered here, $k_0|\beta_{01}^+\beta_{11}^-|^{-1/2}|\Omega_1|/\omega = 0.221$, $k_0|\beta_{01}^+\beta_{11}^-|^{-1/2}|\Omega_2|/\omega = 1.023$, and $k_0|\beta_{01}^+\beta_{11}^-|^{-1/2}|\Omega_3|/\omega = 1.944$). When $|\Omega| > |\Omega_1|$ (all panels in figure 6), backscatter is weak and the wave field over the perturbed depth is dominated by the incident mode-0 edge wave and the forward scattered mode-1 edge wave. This is in marked contrast to the solutions for the same undulating region with no detuning (figure 5*d*), where backscatter is important. In the region $|\Omega_1| < |\Omega| < |\Omega_2|$ (figure 6*a*), the detuning suppresses backscattering but is not large enough to inhibit forward scattering, and energy exchange between the forward modes is nearly complete. Note that the incident wave amplitude is amplified at some locations inside the undulating region. In the region $|\Omega_2| < |\Omega| < |\Omega_3|$ (figure 6*b*), a reduced portion of the incoming mode-0 energy is forward scattered to mode-1, and both $|F_0(Y/L)|^2$ and $|F_1(Y/L)|^2$ oscillatorily approach constants. In the region $|\Omega| > |\Omega_3|$ (figure 6*c*), the amplitudes of these two forward propagating waves oscillate over the perturbed bathymetry. As the detuning

further increases (not shown), both the magnitude and wavelength of the forward amplitude oscillations decrease, indicating the weakening influence of the undulating region.

The variations of normalized energy fluxes outside the undulating region $|F_0(L)|^2$, $|F_1(L)|^2$, $|B_0(0)|^2$, and $|B_1(0)|^2$ as a function of normalized detuning are shown in figure 7. (Recall that $|F_0(0)|^2 = 1$ by definition and that $|F_1(0)|^2 = |B_0(L)|^2 = |B_1(L)|^2 = 0$ from the boundary conditions.) Over a moderately short undulating region (figure 7*a*), the forward scattering to mode 1 that is nearly complete with no detuning is strongly suppressed by increased detuning (i.e. $|F_1(L)|^2$ decreases from approximate unity to near zero with increased detuning). Over long undulating regions the strong backscatter into mode 0 with small detuning weakens with increased detuning (i.e. $|B_0(0)|^2$ decreases from near unity in figures 7*c* and 7*d*). More of the incident energy reaches the downwave region $Y \geqslant L$ as mode-1 and/or as the original mode-0 incident edge wave ($|F_1(L)|^2$ may become zero, see figure 7*c*, *d*). The maximum fraction of energy flux of mode-1 edge wave backscattered to the upwave region is less than about 25% (see the dashed lines in figure 7). For the largest detuning shown in figures 7(*c*) and 7(*d*), resonant scattering is negligible to an observer downwave of the perturbed bathymetry (i.e. $|F_0(L)|^2 \approx 1$, $|F_1(L)|^2 \approx |B_0(0)|^2 \approx |B_1(0)|^2 \approx 0$).

The above results for an incident mode-0 edge wave are now compared with solutions for an incident mode-1 edge wave. Note that for single-wave scattering, exchanging the mode numbers of the incident and scattered waves will not affect the scattering and transmission coefficients, because $\beta_{nm}^{\pm} = \beta_{mn}^{\pm}$ and the square of the effective detuning wavenumber K^2 remains the same (see (3.5) and (3.30)). For example, suppose the resonance condition (2.8) is satisfied for backscattering of mode 0 and 1. The normalized forward and backward energy fluxes with a mode-0 incident wave are identical to those with a mode-1 incident wave, except that in the former case the forward (backward) energy flux pertains to mode 0 (1) and in the latter case to mode 1 (0). This symmetry with respect to the mode numbers of the incident and scattered waves does not hold for multi-wave scattering involving mode 0 and 1. For example, although the variations of $|F_0(L)|^2$ and $|B_0(0)|^2$ with a mode-1 incident wave are identical to those of $|F_1(L)|^2$ and $|B_1(0)|^2$ with a mode-0 incident wave, respectively (cf. figure 8 with 7*d*), they are not identical over the entire undulating region. Moreover, the variations of $|F_1(L)|^2$ and $|B_1(0)|^2$ with a mode-1 incident wave differ significantly from those of $|F_0(L)|^2$ and $|B_0(0)|^2$ with a mode-0 incident wave, respectively, when $k_0|\beta_{01}^{+}\beta_{11}^{-}|^{-1/2}|\Omega|/\omega > 0.221$ (corresponding to $|\Omega| > |\Omega_1|$), especially in the region $1 < k_0|\beta_{01}^{+}\beta_{11}^{-}|^{-1/2}|\Omega|/\omega < 2$ (corresponding to $|\Omega_2| < |\Omega| < |\Omega_3|$).

The multi-wave scattering results presented above are not very sensitive to the particular assumed cross-shore variation of the depth perturbation. Quantitatively similar results are obtained for beach cusps with a range of plausible p and q values (in (4.1) discussed in §4). For bathymetry roughly resembling crescentic bars observed at Duck (see next section), the variations of normalized energy fluxes with a mode-0 or mode-1 incident edge wave are similar to the corresponding results above for beach cusps.

3.3.2. *Over a semi-infinite region*

For small detuning with $0 \leqslant |\Omega| < |\Omega_1|$, $\sigma_+ = \sigma_-^* = \sigma_r + \mathrm{i}\sigma_i$ (σ_r and σ_i are positive real numbers) and the solutions of (2.24) for a semi-infinite region simplify to

$$A_0^+ = \frac{a_0}{2\sigma_r}\left[(\sigma_- + \tilde{\alpha}_0)\mathrm{e}^{i\sigma_r Y} + (\sigma_+ - \tilde{\alpha}_0)\mathrm{e}^{-i\sigma_r Y}\right]\mathrm{e}^{-\sigma_i Y - \mathrm{i}\Omega T}, \tag{3.41a}$$

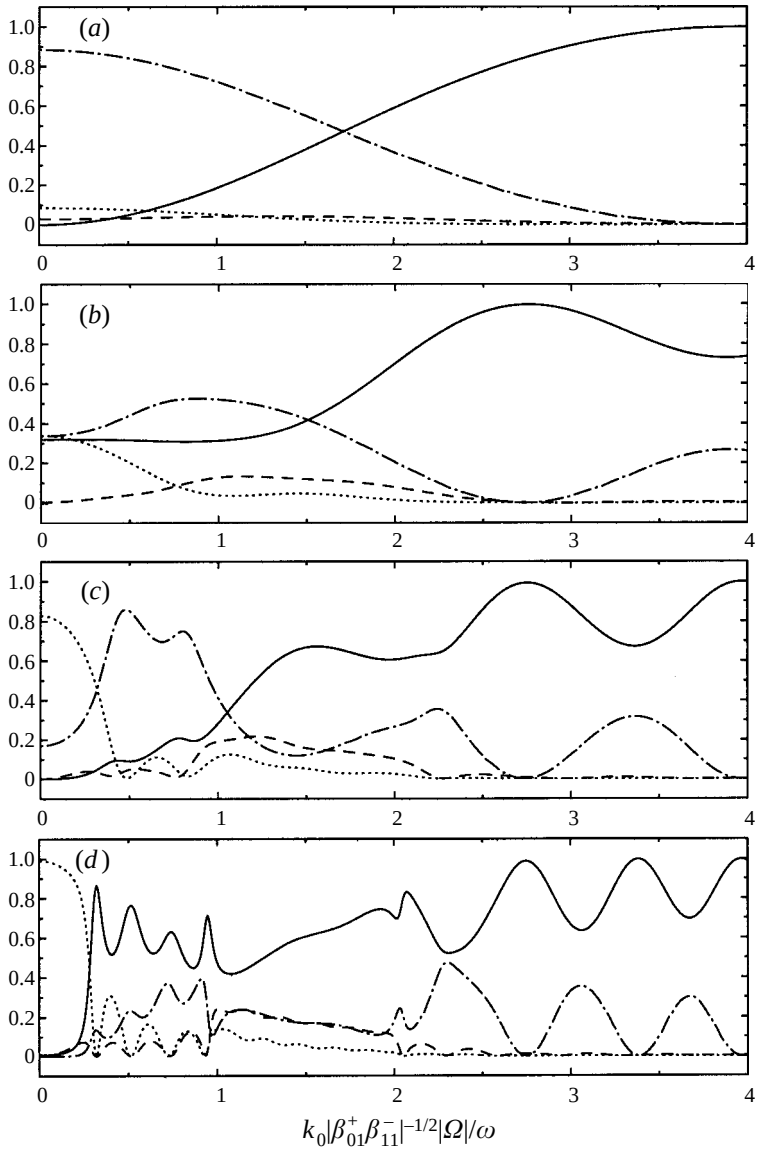

FIGURE 7. Variations of energy fluxes at the edges of the undulating region $Y = 0, L$ (——, $|F_0(L)|^2$; — · —, $|F_1(L)|^2$; · · · ·, $|B_0(0)|^2$; and - - -, $|B_1(0)|^2$) versus the detuning $k_0|\beta_{01}^+\beta_{11}^-|^{-1/2}|\Omega|/\omega$ for different region lengths $|\beta_{01}^+\beta_{11}^-|^{1/2}L = 1.0$ (*a*), 2.5 (*b*), 5.0 (*c*), and 10.0 (*d*). Mode 0 is incident on the cusps so $|F_0(L)|^2 = 1$ corresponds to complete transmission.

$$A_0^- = -\frac{a_0(\beta_{01}^+)^*}{2\sigma_r\beta_{01}^+\beta_{11}^-}\left\{\frac{\sigma_- + \tilde{\alpha}_0}{\sigma_+ + \tilde{\alpha}_0}\left[(\sigma_+ - \tilde{\alpha}_0)(\sigma_+ - \tilde{\alpha}_1) - |\beta_{01}^+|^2\right]\mathrm{e}^{\mathrm{i}\sigma_r Y}\right.$$
$$\left. - \frac{\sigma_+ - \tilde{\alpha}_0}{\sigma_- - \tilde{\alpha}_0}\left[(\sigma_- + \tilde{\alpha}_0)(\sigma_- + \tilde{\alpha}_1) - |\beta_{01}^+|^2\right]\mathrm{e}^{-\mathrm{i}\sigma_r Y}\right\}\mathrm{e}^{-\sigma_i Y - \mathrm{i}\Omega T}, \qquad (3.41b)$$

$$B_0^+ = \mathrm{i}\frac{a_0}{\sigma_r\beta_{01}^+}\frac{C_{g0}}{C_{g1}}(\sigma_+ - \tilde{\alpha}_0)(\sigma_- + \tilde{\alpha}_0)\sin(\sigma_r Y)\mathrm{e}^{-\sigma_i Y - \mathrm{i}\Omega T}, \qquad (3.41c)$$

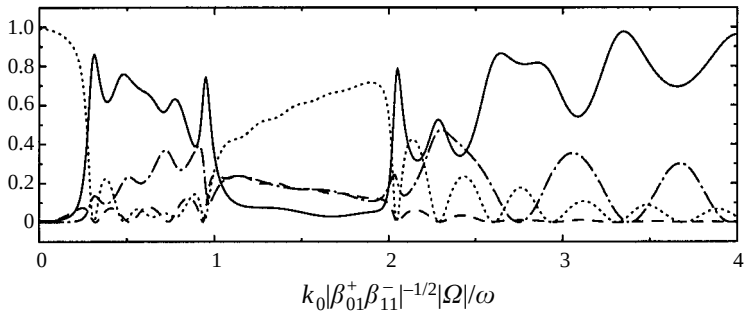

FIGURE 8. Variations of energy fluxes (——, $|F_1(L)|^2$; — · —, $|F_0(L)|^2$; · · · ·, $|B_1(0)|^2$; and - - -, $|B_0(0)|^2$) versus the detuning $k_0|\beta_{01}^+\beta_{11}^-|^{-1/2}|\Omega|/\omega$ with fixed $|\beta_{01}^+\beta_{11}^-|^{1/2}L = 10.0$. Mode 1 is incident on the cusps so $|F_1(L)|^2 = 1$ corresponds to complete transmission. The line types here are such that this figure would be identical to figure 7(*d*) if the normalized energy fluxes were symmetric with respect to mode-0 and mode-1 incident waves.

$$B_0^- = \frac{a_0}{2\sigma_r\beta_{01}^+\beta_{11}^-}\frac{C_{g0}}{C_{g1}}\left\{(\sigma_- + \tilde{\alpha}_0)\left[(\sigma_+ - \tilde{\alpha}_0)(\sigma_+ - \tilde{\alpha}_1) - |\beta_{01}^+|^2\right]\mathrm{e}^{\mathrm{i}\sigma_r Y}\right.$$
$$\left. + (\sigma_+ - \tilde{\alpha}_0)\left[(\sigma_- + \tilde{\alpha}_0)(\sigma_- + \tilde{\alpha}_1) - |\beta_{01}^+|^2\right]\mathrm{e}^{-\mathrm{i}\sigma_r Y}\right\}\mathrm{e}^{-\sigma_i Y - \mathrm{i}\Omega T} \qquad (3.41d)$$

for mode-0 incident waves, and

$$A_0^+ = \mathrm{i}\frac{a_0\beta_{01}^+}{\sigma_r}\frac{C_{g1}}{C_{g0}}\sin(\sigma_r Y)\mathrm{e}^{-\sigma_i Y - \mathrm{i}\Omega T}, \qquad (3.42a)$$

$$A_0^- = -\frac{a_0(\beta_{01}^+)^*}{2\sigma_r\beta_{11}^-}\frac{C_{g1}}{C_{g0}}\left\{(\sigma_+ + \tilde{\alpha}_0)^{-1}\left[(\sigma_+ - \tilde{\alpha}_0)(\sigma_+ - \tilde{\alpha}_1) - |\beta_{01}^+|^2\right]\mathrm{e}^{\mathrm{i}\sigma_r Y}\right.$$
$$\left. + (\sigma_- - \tilde{\alpha}_0)^{-1}\left[(\sigma_- + \tilde{\alpha}_0)(\sigma_- + \tilde{\alpha}_1) - |\beta_{01}^+|^2\right]\mathrm{e}^{-\mathrm{i}\sigma_r Y}\right\}\mathrm{e}^{-\sigma_i Y - \mathrm{i}\Omega T}, \qquad (3.42b)$$

$$B_0^+ = \frac{a_0}{2\sigma_r}\left[(\sigma_+ - \tilde{\alpha}_0)\mathrm{e}^{\mathrm{i}\sigma_r Y} + (\sigma_- + \tilde{\alpha}_0)\mathrm{e}^{-\mathrm{i}\sigma_r Y}\right]\mathrm{e}^{-\sigma_i Y - \mathrm{i}\Omega T}, \qquad (3.42c)$$

$$B_0^- = \frac{a_0}{2\sigma_r\beta_{11}^-}\left\{\left[(\sigma_+ - \tilde{\alpha}_0)(\sigma_+ - \tilde{\alpha}_1) - |\beta_{01}^+|^2\right]\mathrm{e}^{\mathrm{i}\sigma_r Y}\right.$$
$$\left. - \left[(\sigma_- + \tilde{\alpha}_0)(\sigma_- + \tilde{\alpha}_1) - |\beta_{01}^+|^2\right]\mathrm{e}^{-\mathrm{i}\sigma_r Y}\right\}\mathrm{e}^{-\sigma_i Y - \mathrm{i}\Omega T} \qquad (3.42d)$$

for mode-1 incident edge waves ($\tilde{\alpha}_{0,1}$ and $\sigma_\pm$ are defined in (3.33*d*, *e*) and (3.39), respectively). The amplitude of each wave oscillatorily attenuates as Y increases with a decay rate (or e-folding scale) $1/\sigma_i$, where

$$\sigma_i^2 = \tfrac{1}{4}[-\left(\tilde{\alpha}_0^2 + \tilde{\alpha}_1^2 + 2|\beta_{01}^+|^2 - |\beta_{11}^-|^2\right)$$
$$+ 2\left(\tilde{\alpha}_0^2\tilde{\alpha}_1^2 - 2\tilde{\alpha}_0\tilde{\alpha}_1|\beta_{01}^+|^2 - \tilde{\alpha}_0^2|\beta_{11}^-|^2 + |\beta_{01}^+|^4\right)^{1/2}]. \qquad (3.43)$$

It can be shown that backscattering is complete (i.e. $|B_0(0)|^2 + |B_1(0)|^2 = 1$) with a semi-infinite undulating region and weak detuning ($|\Omega| < |\Omega_1|$). For perfect tuning

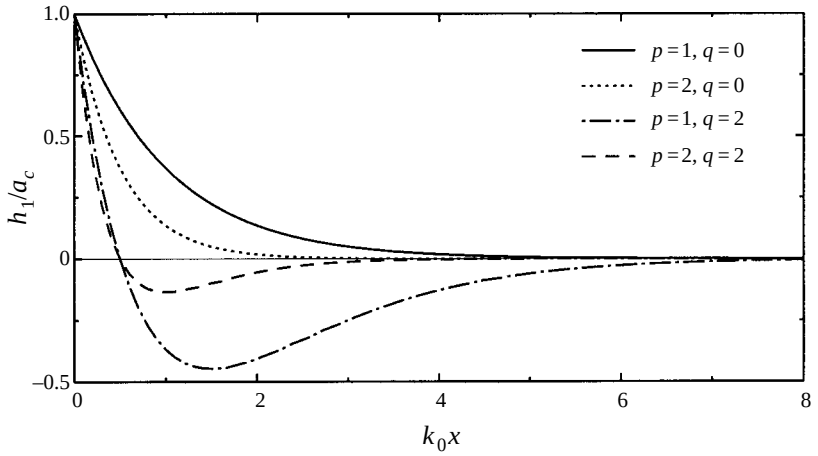

FIGURE 9. Beach cusp profiles (4.1) along cross-shore sections $y = 0, \pm\lambda_c, \pm 2\lambda_c, \ldots$, for different values of p and q.

($\Omega = 0$), two mode-0 edge waves form a standing edge wave, so do two mode-1 edge waves (see figure 5*d*). The e-folding scale in this situation is $1/\sigma_i = 2/|\beta_{11}^-|$, which surprisingly does not depend on β_{01}^+.

4. Scattering by beach cusps and crescentic bars

The scattering of an incident edge wave by longshore periodic bathymetry with dimensions roughly similar to observed beach cusps and crescentic bars is now considered. Coupling coefficients for cusps and crescentic bars are determined first, and then used to show that the amplitudes of these features are large enough to cause strong edge wave scattering, over a significant incident wave frequency bandwidth, within a propagation distance of only $O(10)$ topographic wavelengths.

4.1. *Coupling coefficients for beach cusps*

Cusp-like topographic variations are described as

$$\epsilon h_1(x, y) = a_c\,(1 - qk_0x)\,\mathrm{e}^{-pk_0x}\cos(2\pi y/\lambda_c), \tag{4.1}$$

where a_c and λ_c are the cusp amplitude and cusp wavelength, and $p(>0)$ and $q(\geqslant 0)$ are $O(1)$ constants that alter the exponential offshore decay scale and structure of the cusps (figure 9). With this form for cusps, there is no change in the mean (y-averaged) depth profile (i.e. $c_0 = 0$ in (2.5)). If $c_0 \neq 0$, detuning is altered, but not the coupling coefficient. When $q = 0$, (4.1) is equivalent to the form used by Guza & Bowen (1981). When $q > 0$, $c_1(x)$ changes sign; depth depressions are located offshore of the cusp horns, and deltas are offshore of the cusp bays, as have been occasionally observed (Guza & Inman 1975 and references therein).

For this particular topographic perturbation, the coupling coefficient $\beta_{nm}^{\pm}$ is (from (2.19))

$$\beta_{nm}^{\pm}(p, q) = k_0\bar{n}\bar{m}\Big\{1 - \bar{n}\bar{m}\int_0^{+\infty}(1 - q\chi)\,\big\{\big[L_n'(2\bar{n}\chi) + L_{n+1}'(2\bar{n}\chi)\big] \times \big[L_m'(2\bar{m}\chi) + L_{m+1}'(2\bar{m}\chi)\big] \pm L_n(2\bar{n}\chi)\,L_m(2\bar{m}\chi)\big\}\,\mathrm{e}^{-(p+\bar{n}+\bar{m})\chi}\mathrm{d}\chi\Big\}, \tag{4.2}$$

	B_{00}	B_{01}	M_{01}	F_{02}
$f_0 \times 10$ (Hz)	0.522	0.640	0.905	0.826
l/λ_c	4.1	5.9–9.0	10.8–22.5	13.7–27.9
$\lvert\delta f\rvert/f_0$	0.034	0.015–0.023	0.003–0.006	0.031–0.063

TABLE 1. Low-mode edge wave scattering by beach cusps at Parramore Island. The cusp dimensions are $\lambda_c = 20$ m, $s = 0.07$, and $a_c = 0.035$ m (from Guza & Bowen 1981).

	B_{00}	B_{01}	M_{01}	F_{02}
$f_0 \times 10$ (Hz)	0.604	0.739	1.046	0.954
l/λ_c	2.2	3.1–4.8	5.8–12.0	7.3–15.0
$\lvert\delta f\rvert/f_0$	0.063	0.029–0.044	0.005–0.012	0.058–0.118

TABLE 2. Low-mode edge wave scattering by beach cusps at False Cape. The cusp dimensions are $\lambda_c = 21.4$ m, $s = 0.10$, and $a_c = 0.1$ m (from Guza & Bowen 1981).

where $\bar{n} = (2n+1)^{-1}$, $\bar{m} = (2m+1)^{-1}$, $L_j'(\chi) = \mathrm{d}L_j(\chi)/\mathrm{d}\chi$, and the ordering parameter $\epsilon = a_c k_0/s$ is a measure of the ratio of the mean slope of the cusps to the slope of the unperturbed beach. The integrand in (4.2), consisting of polynomials multiplied by an exponential function, can be evaluated analytically using $\int_0^{+\infty} \chi^j \mathrm{e}^{-\mu\chi}\mathrm{d}\chi = j!/\mu^{j+1}$, where j is a non-negative integer and $\mu > 0$, e.g.

$$\beta_{00}^{-} = k_0, \tag{4.3a}$$

$$\beta_{01}^{-} = \frac{k_0}{3}\left[\frac{3p+2}{3p+4} + \frac{6q}{(3p+4)^2}\right], \quad \beta_{11}^{-} = \frac{k_0}{9}\left[\frac{9p^2+4p+4/3}{(3p+2)^2} + \frac{24pq}{(3p+2)^3}\right], \tag{4.3b,c}$$

$$\beta_{01}^{+} = \frac{k_0}{3}\left[\frac{(3p+2)^2}{(3p+4)^2} + \frac{12q(3p+2)}{(3p+4)^3}\right], \ \beta_{02}^{+} = \frac{k_0}{5}\left[\frac{(5p+4)^3}{(5p+6)^3} + \frac{30q(5p+4)^2}{(5p+6)^4}\right]. \tag{4.3d,e}$$

Note that β_{00}^{-} is independent of the cusp shape parameters p and q, whereas the other $\beta_{nm}^{\pm}$ depend linearly on q. When $q = 0$, $\beta_{nm}^{\pm}$ monotonically increases as p increases and approaches a constant $[(2n+1)(2m+1)]^{-1}k_0$. The inclusion of the term proportional to q increases the value of $\beta_{nm}^{\pm}$ significantly when p is less than 1, but the contribution from this term becomes less significant as p increases. The normalized coupling coefficient $\beta_{nm}^{\pm}/k_0$ decreases as the mode numbers n, m increase due to the factor $[(2n+1)(2m+1)]^{-1}$ (see (4.2)).

The cusp amplitude a_c, wavelength λ_c, and beach slope s observed at Parramore Island and False Cape are given in tables 1 and 2. The frequencies of exact resonance f_0 for single-wave mode-0 Bragg scattering (B_{00}), (0, 1) backward scattering (B_{01}), (0, 2) forward scattering (F_{02}), and (0, 1) multi-wave scattering (M_{01}) are all in the frequency range (0.05–0.10 Hz) of ocean swell (tables 1 and 2). Assume that the shapes of cusps at Parramore Island and False Cape can be described by (4.1) with $\pi/2\lambda_c \leqslant pk_0 \leqslant 5\pi/\lambda_c$ and $0 \leqslant qk_0 \leqslant 2\pi/\lambda_c$ ($k_0 = \omega^2/gs$). From (4.3*b–e*), the minima and maxima of $\beta_{01}^{\pm}$, β_{11}^{-}, and β_{02}^{+} over the corresponding parametric ranges are

$$0.2k_0 \leqslant \beta_{01}^{-} \leqslant 0.307k_0, \quad 0.04k_0 \leqslant \beta_{11}^{-} \leqslant 0.083k_0, \tag{4.4a,b}$$

$$0.103k_0 \leqslant \beta_{01}^{+} \leqslant 0.227k_0, \quad 0.073k_0 \leqslant \beta_{02}^{+} \leqslant 0.148k_0. \tag{4.4c,d}$$

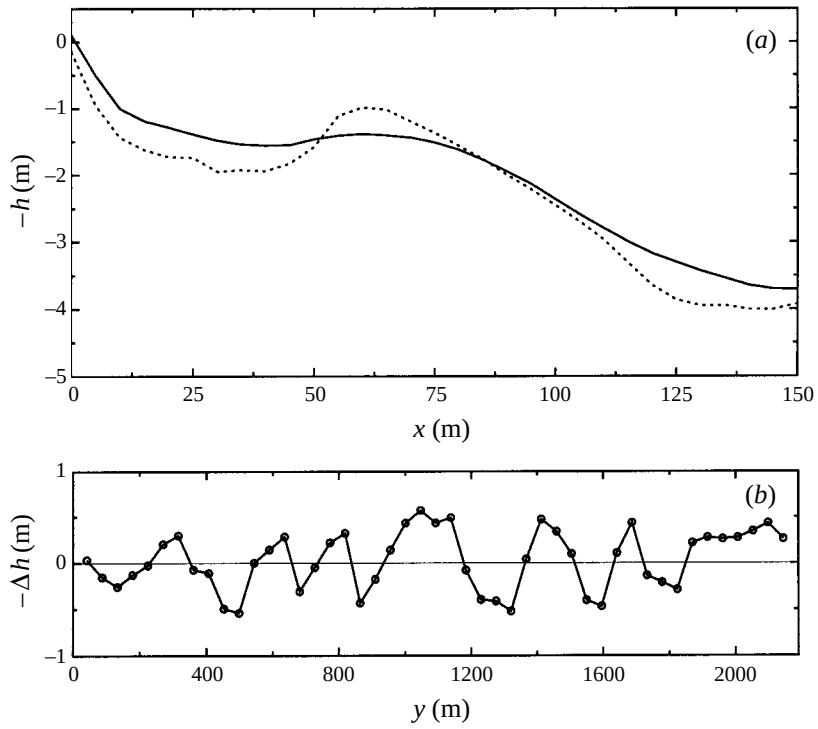

FIGURE 10. Duck bathymetry on 4 December 1996: (*a*) depth profiles along one cross-shore section ($y = 316$ m) ($\cdots$) and averaged over all cross-shore sections (——); (*b*) longshore depth variation (Δh) from the mean depth (about 1.5 m) along one longshore section ($x = 55$ m) (circles indicate the measurement locations).

Normalized (with respect to the cusp wavelength λ_c) e-folding distances l for single-wave backward scattering B_{00}, B_{01}, $l = 1/\epsilon Q$ (see (3.19)), and multi-wave scattering M_{01}, $l = 1/\epsilon\sigma_i$ (see (3.43)), and the envelope wavelength for forward scattering F_{02}, $l = \pi/\epsilon P$ (see (3.32)), assuming no frequency detuning and that cusps extend over a large longshore distance, are shown in tables 1 and 2 (second row). At resonance, single-wave backscattering is very strong and e-folding scales are generally less than $10\lambda_c$. Multi-wave scattering and forward scattering are slightly weaker (the e-folding scale and the envelope wavelength are $O(10)\lambda_c$). The frequency detuning $|\delta f|/f_0$ shown in the tables corresponds to doubling these e-folding distances and reducing the maximum forward scattering coefficient from 1 to 1/2 (see (3.32)). The relatively narrow bandwidth for multi-wave scattering indicates that detuning more strongly affects multi-wave scattering than single-wave scattering. Owing to uncertainty in the estimates of p and q (Guza & Bowen 1981), a range of l/λ_c and $|\delta f|/f_0$ values (corresponding to the upper and lower bounds of $\beta_{01}^{\pm}$, β_{11}^{-}, and β_{02}^{+} given in (4.4)) are given for B_{01}, M_{01}, and F_{02} (B_{00} is independent of p and q).

Over a propagation distance of $O(10)$ cusp wavelengths most of the energy of an incident plane wave (with frequency deviation from f_0 less than $|\delta f|$) will be scattered to edge waves propagating in either the same or opposite direction. In fact, the predicted mode-0 single-wave backscattering is so strong (e.g. e-folding distance of about $2.2\lambda_c$ at False Cape) that the slowly varying assumption of the theory is probably violated.

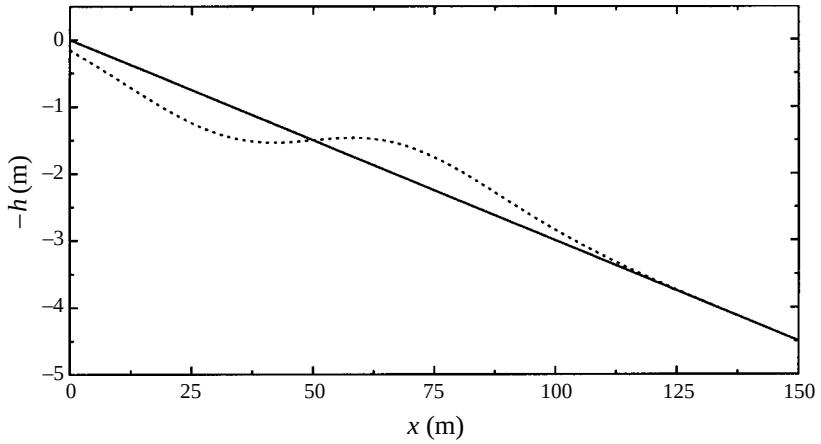

FIGURE 11. The mean depth profile (——) and profile (····) along cross-shore sections $y = j\lambda_c\,(j = 0, \pm 1, \ldots)$ of the crescentic sandbar given by (4.5) with $s = 0.03$, $a_c = 0.5$ m, $b = 50$ m, $c = 0.0314$ m^{-1}, and $\lambda_c = 250$ m.

4.2. *Coupling coefficients for crescentic sandbars*

Crescentic sandbars have wavelengths (typically several 100 m, Lippmann & Holman 1990) longer than beach cusps, and therefore scatter lower-frequency edge waves than cusps. Bathymetric surveys at Duck, NC spanning 2 km alongshore (figure 10) are used to illustrate the potential effect of a field-scale crescentic bar on edge wave propagation. The depth deviation (from the mean beach profile, figure 10*a*) varied periodically with longshore wavelength about 250 m and amplitude about 0.5 m (figure 10*b*).

A crescentic sandbar superposed on a uniform plane beach is represented as

$$h = sx + \epsilon h_1 = sx + a_c(2\mathrm{e})^{1/2}c(x-b)\mathrm{e}^{-[c(x-b)]^2}\cos(2\pi y/\lambda_c), \tag{4.5}$$

where a_c is the maximum deviation of the sandbar from the plane beach, b is the cross-shore location of zero perturbation (note that h_1 given by (4.5) is antisymmetric about $x = b$), c controls the width of the sandbar about the centre, and λ_c is the sandbar longshore wavelength. Using selected values of these parameters the depth deviation from the plane beach given in (4.5) crudely resembles the deviation of the Duck bathymetry from the mean Duck profile (compare figure 11 with figure 10*a*). The shape of ϵh_1 given in (4.5) is also close to that of the resonant Fourier component $c_1(x)\cos(2\pi y/\lambda_c)$ of a symmetric 'hump' sandbar wiggling between $x = b - d$ and $x = b + d$ (e.g. $\epsilon h_1(x, y) = a_c G\left(c[x - b + d\cos(2\pi y/\lambda_c)]\right)$ with $G(x) = 1/(1 + x^2)$, $\mathrm{sech}(x)$, or $\exp(-x^2)$).

The coupling coefficient $\beta^{\pm}_{nm}$ corresponding to the sandbar (4.5) is

$$\beta^{\pm}_{nm}(\tilde{b}, \tilde{c}) = -(2\mathrm{e})^{1/2}k_0\tilde{c}\mathrm{e}^{-\tilde{b}^2\tilde{c}^2}\bar{n}\bar{m}\Bigg\{\tilde{b} + \bar{n}\bar{m}\int_0^{+\infty}(\chi - \tilde{b})\left\{\left[L'_n(2\bar{n}\chi) + L'_{n+1}(2\bar{n}\chi)\right]\right.$$
$$\left.\times\left[L'_m(2\bar{m}\chi) + L'_{m+1}(2\bar{m}\chi)\right] \pm L_n(2\bar{n}\chi)\,L_m(2\bar{m}\chi)\right\}\mathrm{e}^{-\tilde{c}^2\chi^2 + (2\tilde{b}\tilde{c}^2 - \bar{n} - \bar{m})\chi}\mathrm{d}\chi\Bigg\}, \tag{4.6}$$

where $\tilde{b} = bk_0$, $\tilde{c} = c/k_0$, $\bar{n} = (2n+1)^{-1}$, $\bar{m} = (2m+1)^{-1}$, and the ordering parameter

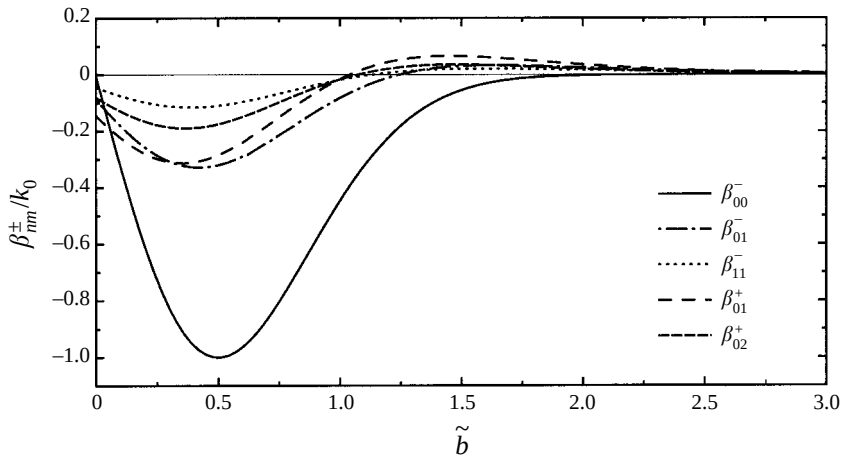

FIGURE 12. Normalized coupling coefficients β_{00}^{-}, $\beta_{01}^{\pm}$, β_{11}^{-}, and β_{02}^{+} (see (4.7)) versus the normalized bar shape parameter $\tilde{b}$ for $\tilde{c} = 2^{1/2}$.

ϵ is again $a_c k_0/s$. The integral in (4.6) can be evaluated in terms of the error function $\mathrm{erf}(q) = 2\pi^{-1/2}\int_0^q \mathrm{e}^{-\chi^2}\mathrm{d}\chi$, e.g.

$$\beta_{00}^{-} = -(2\mathrm{e})^{1/2} k_0 \tilde{b}\tilde{c}\mathrm{e}^{-\tilde{b}^2\tilde{c}^2}, \tag{4.7a}$$

$$\beta_{01}^{-} = \frac{\beta_{00}^{-}}{3}\left\{1 + \frac{1}{3\tilde{b}\tilde{c}^2}\left[1 - \frac{2\pi^{1/2}}{3\tilde{c}}\mathrm{e}^{\tau_1^2}\left[1 + \mathrm{erf}(\tau_1)\right]\right]\right\}, \tag{4.7b}$$

$$\beta_{11}^{-} = \frac{\beta_{00}^{-}}{9}\left\{1 + \frac{4}{9\tilde{b}\tilde{c}^2}\left[1 + \frac{1}{9\tilde{c}^2} - \frac{\pi^{1/2}}{\tilde{c}}\left(\frac{1}{2} - \frac{\tilde{b}}{9} + \frac{1}{27\tilde{c}^2}\right)\mathrm{e}^{\tau_2^2}\left[1 + \mathrm{erf}(\tau_2)\right]\right]\right\}, \tag{4.7c}$$

$$\beta_{01}^{+} = \frac{\beta_{00}^{-}}{3}\left\{1 + \frac{2}{3\tilde{b}\tilde{c}^2}\left[1 + \frac{2}{9\tilde{c}^2} - \frac{\pi^{1/2}}{\tilde{c}}\left(\frac{5}{6} - \frac{2\tilde{b}}{9} + \frac{4}{27\tilde{c}^2}\right)\mathrm{e}^{\tau_1^2}\left[1 + \mathrm{erf}(\tau_1)\right]\right]\right\}, \tag{4.7d}$$

$$\beta_{02}^{+} = \frac{\beta_{00}^{-}}{5}\left\{1 + \frac{1}{25\tilde{b}\tilde{c}^4}\left[4 + \frac{18}{5^3\tilde{c}^2} + 15\tilde{c}^2 - \frac{6\tilde{b}}{25} - \frac{\pi^{1/2}}{\tilde{c}}\left(\frac{63}{25} + \frac{54}{5^4\tilde{c}^2} + 12\tilde{c}^2 - \frac{36\tilde{b}}{5^3} - 4\tilde{b}\tilde{c}^2 + \frac{6}{25}\tilde{b}^2\tilde{c}^2\right)\mathrm{e}^{\tau_3^2}\left[1 + \mathrm{erf}(\tau_3)\right]\right]\right\}, \tag{4.7e}$$

where

$$\tau_1 = \tilde{b}\tilde{c} - 2/3\tilde{c}, \quad \tau_2 = \tilde{b}\tilde{c} - 1/3\tilde{c}, \quad \tau_3 = \tilde{b}\tilde{c} - 3/5\tilde{c}. \tag{4.8}$$

Figure 12 shows β_{00}^{-}, $\beta_{01}^{\pm}$, β_{11}^{-}, and β_{02}^{+} (normalized by k_0) as a function of $\tilde{b}$ for fixed $\tilde{c} = 2^{1/2}$ (at Duck $\tilde{c} = 2.50$, 1.67, 1.00, and 0.83 for B_{00}, B_{01}, F_{02}, and M_{01}, respectively). For different values of $\tilde{c}$, due to the factor $\mathrm{e}^{-\tilde{b}^2\tilde{c}^2}$, the shapes of these curves remain almost the same with an inversely proportional stretching (compressing) of the $\tilde{b}$-axis. The maximum is achieved near $\tilde{b} = (2\tilde{c}^2)^{-1/2}$, corresponding to the situation where the sandbar has the maximum depth perturbation at the shoreline $x = 0$. The coupling coefficient exponentially decays for large $\tilde{b}$ (i.e. a sandbar far from the shoreline has no effect on edge wave propagation) and also decays as $\tilde{b}$ decreases (when $\tilde{b} = b = 0$, the depth perturbation at the shoreline vanishes). The maximum value of $|\beta_{nm}^{\pm}|/k_0$ decreases as n and m increase, again due to the factor $[(2n+1)(2m+1)]^{-1}$ in (4.6).

	B_{00}	B_{01}	M_{01}	F_{02}
$f_0 \times 10$ (Hz)	0.097	0.118	0.168	0.153
l/λ_c	4.9	14.5	21.0	38.8
$\lvert\delta f\rvert/f_0$	0.028	0.010	0.003	0.022

TABLE 3. Low-mode edge wave scattering by an semi-infinitely long field of crescentic sandbars. The sandbar dimensions in (4.5) are $s = 0.03$, $a_c = 0.5$ m, $b = 50$ m, $c = 0.0314$ m^{-1}, and $\lambda_c = 250$ m.

For the crescentic bar shape (4.5) with observation-based parameter values (figure 11), the values of low-mode coupling coefficients normalized by k_0 are: $\beta_{00}^{-}/k_0 = -0.3102$, $\beta_{01}^{-}/k_0 = -0.0466$, $\beta_{11}^{-}/k_0 = 0.0161$, $\beta_{01}^{+}/k_0 = 0.0468$, and $\beta_{02}^{+}/k_0 = 0.0197$. Table 3, corresponding to tables 1 and 2, gives the infragravity wave frequencies (f_0) for resonant scattering, normalized e-folding distances (for B_{00}, B_{01}, and M_{01}) (l/λ_c) and envelope wavelength (for F_{02}) (l/λ_c) with perfect tuning, and the frequency detuning ($|\delta f|/f_0$) to double these e-folding lengths and reduce the envelope amplitude by half. Although the resonant frequencies for scattering by crescentic bars (table 3) are roughly a factor of 5 lower than the corresponding resonant frequencies for scattering by cusps (tables 1 and 2), their normalized e-folding and detuning values are similar.

4.3. *Backscattering of waves with finite bandwidth*

Here we estimate the fraction of an incident edge wave spectrum with finite bandwidth that is backscattered by a finite number of periodic cusps and crescentic bars. The incident edge wave spectral level $P(f)$ is assumed constant over $[f_0 - \Delta f, f_0 + \Delta f]$, where f_0 is the exactly resonant frequency. The cusp topography is given by (4.1) with $pk_0 = \pi/\lambda_c$ and $q = 0$, and the cusp wavelength, cusp amplitude, and mean beach slope by the Parramore observations (table 1). The crescentic bar parameters are based on (4.5) and the Duck observations (table 3). Two different lengths of undulating region, 20 and 40 wavelengths (λ_c) of the rhythmic topography, are considered. The total frequency-integrated backward scattering coefficient at $Y = 0$, the upwave end of the perturbed bathymetry, is defined as

$$|S_t(\Delta f)|^2 = \int_{f_0-\Delta f}^{f_0+\Delta f} P(f)|S(f)|^2 \mathrm{d}f \Big/ \int_{f_0-\Delta f}^{f_0+\Delta f} P(f)\mathrm{d}f, \tag{4.9}$$

where $|S(f)|^2$ is the total squared scattering coefficient at $Y = 0$ corresponding to an incident edge wave with a near-resonant, monochromatic frequency f. For single-wave backscattering, $|S(f)|^2$ is given by (3.9), (3.12), or (3.15), depending on whether the detuning is subcritical, critical, or supercritical. For (0, 1) multi-wave scattering, $|S(f)|^2 = |B_0(0)|^2 + |B_1(0)|^2$ is the sum of the normalized mode-0 and mode-1 backscattered fluxes. Numerical integration of (4.9) (note that $P(f)$ drops out of (4.9) since it is assumed constant over $[f_0 - \Delta f, f_0 + \Delta f]$) yields $|S_t|^2$, the fraction of the incident wave energy that is backscattered, as a function of the spectral bandwidth Δf about the resonant frequency f_0. The same procedure can be used to find the total band-integrated forward scattering coefficient. Results corresponding to (0, 0), (0, 1), (0, 2), and (1, 2) single-wave backscattering and (0, 1) multi-wave scattering (with a mode-1 incident edge wave) for the Parramore beach cusps and the Duck crescentic bar are shown in figures 13 and 14. Note that $|S_t(\Delta f)|^2$ at $f = f_0 \pm \Delta f$, where f is the frequency variable in the figures, is the backscattered fraction of a spectrum that is

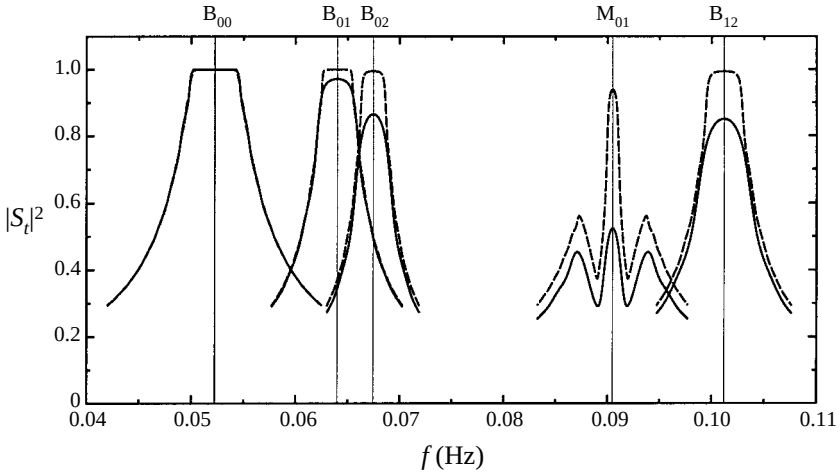

FIGURE 13. The integrated backward scattering coefficient $|S_t|^2$ for Parramore beach cusps (table 1) versus Δf (4.9), where Δf is the deviation of f from the resonant frequency f_0 (f_0 for (0, 0), (0, 1), (0, 2), (1, 2) single-wave backscattering, and (0, 1) multi-wave scattering are indicated by the thin vertical lines). Results are shown for different longshore lengths of the undulating region: $20\lambda_c$ (solid lines) and $40\lambda_c$ (broken lines), where $\lambda_c = 20$ m is the cusp wavelength.

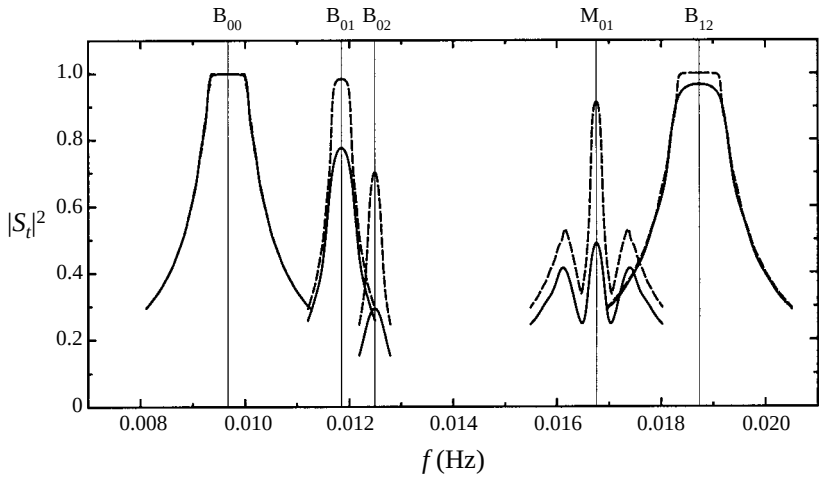

FIGURE 14. Same as figure 13, but for the crescentic bar given by (4.5) and table 3.

white between $f_0 - \Delta f$ and $f_0 + \Delta f$, with f_0 the frequency of exact resonance indicated by vertical lines.

For single-wave backscattering, the maximum bandwidth considered in figures 13 and 14 is $(\Delta f)_{\max} = 5\Delta f_c$, where $\Delta f_c = \epsilon f_0 |\beta_{nm}^-|/k_t$ is the critical bandwidth within which the detuning is subcritical. Note that $\Delta f_c = 2|\delta f|/\sqrt{3}$, where $|\delta f|$ is the detuning frequency (given in tables 1–3) needed to double the e-folding scale on a semi-infinite undulating patch. Within the critical bandwidth, detuning is weak and backscattering is strong (also see figure 3), so the band-integrated scattering coefficient $|S_t|^2$ is insensitive to the variation of the frequency bandwidth Δf (figures 13 and 14). As the frequency bandwidth of the incident wave increases beyond critical, backscattering is much weaker (figure 3) and $|S_t|^2$ decays rapidly. The scattering coefficient $|S_t|^2$ is insensitive to the length L of the perturbed region when $\Delta f > \Delta f_c$, but within the

critical bandwidth ($\Delta f < \Delta f_c$), $|S_t|^2$ increases noticeably as L increases (from $20\lambda_c$ to $40\lambda_c$) before reaching 1 (complete scattering). For the (0, 1) multi-wave scattering, the maximum bandwidth considered in figures 13 and 14 is $(\Delta f)_{\max} = 5\epsilon f_0|\beta_{11}^-|/k_t$. As the bandwidth Δf increases, $|S_t|^2$ first rapidly decreases, then increases, and finally decreases again (consistent with the variation of $|B_1(0)|^2$ with detuning in figure 8). Strong backscattering ($|S_t|^2 > 0.5$) occurs only for incident waves with a relatively narrow bandwidth propagating over a corrugated region longer than 20 topographic wavelengths.

For the Parramore beach cusps (figure 13), the regions of significant ($|S_t|^2 > 0.3$) scattering centred at the resonant frequencies f_0 for (0, 0), (0, 1), and (0, 2) backscattering overlap. Thus, more than 30% of the energy of incident mode-0 edge waves, with a white spectrum spanning the frequency range of the overlapping resonances (roughly 0.045–0.07 Hz), is theoretically backscattered. Similarly, significant backscattering by the Parramore cusps is predicted for mode-1 incident edge waves in the frequency range approximately 0.085–0.105 Hz (figure 13), and by the Duck crescentic bar for infragravity edge waves (e.g. mode-0 edge waves in 0.008–0.012 Hz and mode-1 edge waves in 0.016–0.02 Hz) (figure 14). In these cases of overlapping resonances, the present theory should be modified to allow simultaneous energy transfer among several waves involved. For example at Parramore beach, the amplitudes of a 0.066 Hz, mode-0 incident wave, and mode-1 and mode-2 backscattered edge waves should be all coupled. The resulting equations are similar to the multi-wave scattering equations (2.24), but are a generalization in that the resonant frequencies of the simultaneously occurring resonances need not coincide and can differ by a small amount.

5. Discussion

5.1. *Scattering by bathymetry with finite bandwidth*

The total scattering coefficient for an edge wave with finite bandwidth propagating over bathymetry with a single wavenumber was obtained through linear superposition (see (4.9)) of the results for a monochromatic wave given in §3. This is possible because each (assumed) linear wave component independently interacts with the perturbed bottom. However, the total scattering coefficient for a monochromatic wave propagating over a perturbed depth with finite bandwidth cannot be obtained by superposition, because (near resonance) the scattering coefficients are not linearly proportional to the amplitude of the topographic undulations c_1 (although the coupling coefficient $\beta_{nm}^{\pm}$ (2.19) depends linearly on c_1, the scattering coefficients, e.g. (3.7), are not linear functions of $\beta_{nm}^{\pm}$). Scattering by all bottom components must be considered simultaneously.

To model the scattering of a monochromatic incident wave by bathymetry with a near-resonant bandwidth $[k_t - \epsilon\tilde{K}, k_t + \epsilon\tilde{K}]$ ($\tilde{K}$ is an $O(k_t)$ constant), divide the bathymetric wavenumber spectrum $P_B(k; x)$ in the near-resonant bandwidth into $2J$ subintervals with resolution $\Delta k = \epsilon\tilde{K}/J$. Express the perturbed depth as a slowly modulated sinusoidal perturbation

$$h_1 = \sum_{j=-J}^{j=J} b_j(x)\cos\left[(k_t + j\Delta k)y + \phi_j\right]$$
$$= \tfrac{1}{2}e^{ik_t y}\sum_{j=-J}^{j=J} b_j(x)e^{i(j\tilde{K}Y/J+\phi_j)} + * = c_B(x, Y)e^{ik_t y} + *, \tag{5.1}$$

where $b_j = \{2P_B(k_t + j\Delta k; x)\Delta k\}^{1/2}$, $c_B(x, Y) = \frac{1}{2}\sum_{j=-J}^{j=J} b_j(x)e^{i(j\tilde{K}Y/J+\phi_j)}$ is complex, and ϕ_j are phases. Replacing c_1 with c_B in (2.19) and substituting the resulting coupling coefficient into (2.16) or (2.24) yields coupled variable-coefficient equations for single-wave or multi-wave scattering of a monochromatic wave propagating over a perturbed bed with a near-resonant bandwidth and fixed phases ϕ_j. If the bathymetry is assumed to have random rather than deterministic phases, the results of many phase realizations can be averaged together. Development of a theory for the scattering of a spectrum of edge waves by a spectrum of bathymetric undulations is beyond the scope of the present work.

5.2. *Morphology formation*

Consider single-wave scattering over pre-existing longshore periodic bathymetry. Theoretically, the incident and phase-locked scattered edge waves produce a longshore periodic steady drift velocity (Bowen & Inman 1971; Holman & Bowen 1982). The longshore wavenumber of the drift velocity coincides with the wavenumber of the existing perturbed topography. Consequently, the sediment transport driven by the drift velocity may alter the amplitude of the existing longshore periodic topography and/or extend upwave the spatial extent of the rhythmic morphology if it has an appropriate phase relation to the pre-existing topography. For perfect tuning ($K = 0$) and a sufficiently long undulating region, the phase difference ($-\pi/2$) in (3.21) indicates that nodes and antinodes of standing waves formed by backscattering occur at midpoints between adjacent extrema of the perturbed depth h_1. However, models for morphology formation suggest that extrema of the morphology form at standing edge wave nodes and antinodes. Further work is needed to determine if a pre-existing morphology is reinforced, eroded, or moved by standing waves formed by backscattering.

If the feedback between the resonantly scattered waves and the morphology is constructive, then backscattering of waves with the same wavenumber as the incident waves provides a mechanism for forming a field of rhythmic shoreline parallel features (e.g. cusps and regular crescentic bars). Scattering of phase-coupled edge waves with different wavenumbers may result in oblique sandbars welded to the shoreline (Holman & Bowen 1982). For multi-wave scattering, the interaction of incident and phases-locked scattered (more than one) edge waves may produce 'bars, bumps, and holes' with more complex shapes (Holman & Bowen 1982).

6. Summary

Resonant scattering of progressive low-mode edge waves by longshore periodic topography is investigated theoretically using a multiple-scale expansion of the linear shallow water equations. In 'single-wave scattering', an incident edge wave is resonantly forward or backward scattered by the periodic topography into a single additional progressive edge wave of the same frequency. Backscattering into an edge wave with the same mode number (i.e. longshore wavenumber) as the incident edge wave, the analogue of Bragg scattering of surface waves in constant depth, is a special case. In 'multi-wave scattering', simultaneous forward and backward resonant scattering results in several (rather than only one) new progressive edge waves. Coupled evolution equations for the slowly varying amplitudes of incident and scattered edge waves show that resonant scattering depends on both the longshore wavenumber and cross-shore structure of the perturbed depth and of the incident and scattered waves. For single-wave backward scattering with small (subcritical) detuning from exact

resonance, the incident and backscattered wave amplitudes both exponentially decay over the undulating bathymetry, and backscattering is nearly complete over a sufficiently long undulating region (figures 1 and 3). On the other hand, when the detuning is relatively large (supercritical), the wave amplitudes oscillate over the corrugated region (figure 2). Although backscattering is incomplete with supercritical detuning (figure 3), in some circumstances the incident and backscattered wave amplitudes are significantly amplified at some locations within the undulating region (figure 2). For single-wave forward scattering, the amplitudes of both waves oscillate over the perturbed depth irrespective of the magnitude of the detuning (see (3.32)). Increasing detuning reduces the magnitude and wavelength of the amplitude oscillations. For the special case of multi-wave scattering involving mode-0 and mode-1 edge waves considered here, the variations of the incident and scattered wave amplitudes over the perturbed bathymetry are complex and strongly depend on the frequency detuning (figures 5 and 6). With small detuning, most of the incident wave energy is reflected from a long undulating region (figures 7*d* and 8).

These results are used to show that longshore periodic bathymetry roughly resembling observed beach cusps and crescentic bars can scatter significant amounts of low-mode edge wave energy (most of the energy of a monochromatic incident edge wave at the resonant frequency will be scattered over a distance of $O(10)$ topographic wavelengths). The width of the frequency band (about the resonant frequency) that is significantly scattered is substantial. For example, well developed beach cusps measured at one ocean beach are predicted to strongly backscatter mode-0 edge waves in a frequency band 0.045–0.07 Hz that includes much of the frequency range of ocean swell (figure 13).

This research was supported by the Mellon Foundation and the Office of Naval Research (Coastal Dynamics). We thank the staff of the US Army Corps of Engineers Field Research Facility for providing the crescentic sandbar profiles at Duck, NC.

Appendix A. Effect of a slowly varying slope on single-wave resonant scattering

The case where the slope of the unperturbed beach s varies slowly in the longshore direction is examined for single-wave scattering. According to the dispersion relation (2.9), the wavenumbers (k_n and k_m) and group velocities (C_{gn} and C_{gm}) also vary slowly in the longshore direction. To enable analytic results, perfect tuning is assumed, i.e. the mean (y-averaged) profile does not deviate from the plane beach ($c_0 = 0$) and frequency detuning vanishes everywhere ($\Omega = 0$). In other words, it is assumed that the wavenumber of the bathymetry varies alongshore so that (2.8) is satisfied and exact resonance is maintained as the mean beach slope s and edge wave wavenumbers change. In this case, (2.16) for single-wave scattering simplifies to

$$\bar{A}_Y = \mathrm{i}\beta^{\pm}_{nm}\bar{B}, \quad \pm\bar{B}_Y = \mathrm{i}(\beta^{\pm}_{nm})^*\bar{A}, \tag{A 1}$$

where

$$\bar{A} = C_{gn}A_0, \quad \bar{B} = C_{gm}B_0. \tag{A 2}$$

Considering a finite undulating region $0 \leqslant Y \leqslant L$, assuming $c_1 = c_1(k_0x)$ (i.e. the cross-shore shape of the rhythmic topography scales with the evolving topographic

wavenumber, as in the case in (4.1)), and (for analytic convenience) letting the slope vary as

$$s = s_0(1 + s_1 Y)^{1/3}, \quad 0 \leqslant Y \leqslant L, \tag{A 3}$$

where $s_0(> 0)$ and $s_1(> -L^{-1})$ are constants, yields (see (2.19))

$$\beta^{\pm}_{nm}(Y) = \beta^{\pm}_{nm}(0)/(1 + s_1 Y), \quad 0 \leqslant Y \leqslant L. \tag{A 4}$$

Combining the equations in (A 1) gives

$$(1 + s_1 Y)^2 \bar{A}_{YY} + s_1(1 + s_1 Y)\bar{A}_Y \pm |\beta^{\pm}_{nm}(0)|^2 \bar{A} = 0, \quad 0 \leqslant Y \leqslant L. \tag{A 5}$$

For backward resonant scattering, the wave fields over the corrugated region are given by

$$A_0 = a_0 \left[C_{gn}(0)/C_{gn}(Y)\right] T(Y), \quad B_0 = a_0 \left[C_{gn}(0)/C_{gm}(Y)\right] S(Y), \quad 0 \leqslant Y \leqslant L, \tag{A 6}$$

with

$$T(Y) = \frac{(1 + s_1 Y)^{|\gamma^-_{nm}|} + (1 + s_1 L)^{2|\gamma^-_{nm}|}(1 + s_1 Y)^{-|\gamma^-_{nm}|}}{1 + (1 + s_1 L)^{2|\gamma^-_{nm}|}}, \tag{A 7a}$$

$$S(Y) = -\mathrm{i}|\gamma^-_{nm}| \frac{(1 + s_1 Y)^{|\gamma^-_{nm}|} - (1 + s_1 L)^{2|\gamma^-_{nm}|}(1 + s_1 Y)^{-|\gamma^-_{nm}|}}{\gamma^-_{nm}\left[1 + (1 + s_1 L)^{2|\gamma^-_{nm}|}\right]}, \tag{A 7b}$$

where a_0 is the incident wave amplitude at $Y = 0$ and $\gamma^-_{nm} = \beta^-_{nm}(0)/s_1$. For forward resonant scattering, the wave fields over the undulating region are given by (A 6) with

$$T(Y) = \cos\left[|\gamma^+_{nm}| \ln(1 + s_1 Y)\right], \; S(Y) = \mathrm{i}(\gamma^+_{nm})^{-1}|\gamma^+_{nm}| \sin\left[|\gamma^+_{nm}| \ln(1 + s_1 Y)\right], \tag{A 8}$$

where $\gamma^+_{nm} = \beta^+_{nm}(0)/s_1$. As $s_1 \to 0$, $T(Y)$ and $S(Y)$ in (A 7) and (A 8) approach (3.10) and (3.28) with $K = 0$ for constant slope, respectively.

Figure 15 shows the dependence of the squared backscattering coefficient $|S(0)|^2$ (A 7*b*) on $|\beta^-_{nm}(0)|L$ and $s_1 L$ (note that the relative change of slope over the entire undulating region $[0, L]$ is $[(1 + s_1 L)^{1/3} - 1]$). For fixed $|\beta^-_{nm}(0)|L$, $|S(0)|^2$ decreases with increasing $s_1 L$. For fixed $s_1 L$, $|S(0)|^2$ monotonically increases with increasing $|\beta^-_{nm}(0)|L$, and approaches 1 faster (more slowly) for decreasing (increasing) slope than for constant slope. Thus, over a fixed distance L, more wave energy is backscattered due to the increase of the coupling coefficient (A 4) when the mean slope in the undulating region decreases, whereas less energy is backscattered due to the decrease of the coupling coefficient (A 4) when the slope increases. Note that although the group velocities C_{gn} and C_{gm} also alter over a slowly varying slope, they will not affect the scattering and transmission coefficients (see (A 1), and note that $|\bar{A}|^2 = a_0^2 C_{gn}^2(0)|T|^2$ and $|\bar{B}|^2 = a_0^2 C_{gn}^2(0)|S|^2$).

The forward scattering coefficient

$$|S(Y)|^2 = \sin^2\left[|\beta^+_{nm}(0)|Y \frac{\ln(1 + s_1 Y)}{|s_1|Y}\right], \quad 0 \leqslant Y \leqslant L, \tag{A 9}$$

oscillates between 0 and 1 because perfect tuning is maintained, but the envelope wavenumber varies (compare (A 9) with (3.32) at $K = 0$). The envelope wavenumber decreases as the slope increases ($s_1 > 0$), and increases as the slope decreases ($s_1 < 0$).

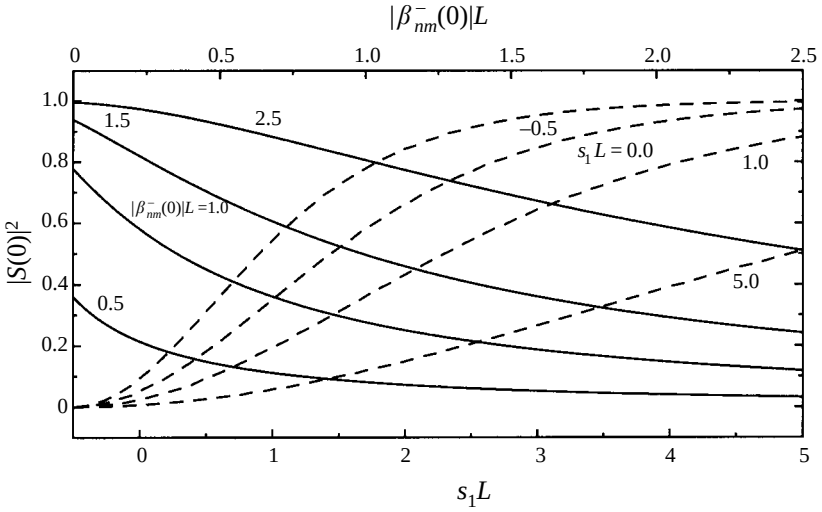

FIGURE 15. The effect of the slowly varying slope (A 3) on the squared backward scattering coefficient at $Y = 0$. For —— (- - -) refer to the bottom (top) of the figure for abscissa.

Note that for backscattering, if the frequency detuning is non-zero, i.e. $\Omega \neq 0$, the corresponding effective detuning wavenumber can be written as $|K|^2 = (\Omega/C_{gn} + \Omega/C_{gm})^2/4 = |K(0)|^2/(1+s_1Y)^{2/3}$. The ratio $|K|^2/|\beta^-_{nm}|^2 = (1+s_1Y)^{4/3}|K(0)|^2/|\beta^-_{nm}(0)|^2$ increases (decreases) as the slope increases (decreases) over the corrugated region $[0, L]$. Therefore, an incident wave that is subcritical (supercritical) entering an undulating region with increasing (decreasing) slope, may cross the critical detuning within the undulating region and becomes supercritical (subcritical), dramatically changing the behaviour of the wave field. Numerical solutions of the variable-coefficient coupled equations (2.16) are straightforward but are not pursued here.

Appendix B. Counter-propagating edge waves over an infinite undulating region

Consider two counter-propagating edge waves with the same mode number n propagating over an infinitely long region of perturbations with wavenumber k_t. Multi-wave cases are excluded so $n \neq 1, 4$, etc. In this situation, there is no spatial variation in wave amplitudes so $\partial_Y = 0$ in (2.16), and the corresponding $O(\epsilon^0)$ free surface displacement (2.10) is

$$\eta_0 = \varphi_n \left[C_1 e^{i(\alpha_n+|\beta^-_{nn}|)C_{gn}T} + C_2 e^{i(\alpha_n-|\beta^-_{nn}|)C_{gn}T}\right] e^{i(k_n y-\omega t)} + \varphi_n e^{-i\theta}\left[C_1 e^{i(\alpha_n+|\beta^-_{nn}|)C_{gn}T} - C_2 e^{i(\alpha_n-|\beta^-_{nn}|)C_{gn}T}\right] e^{i(-k_n y-\omega t)} + *, \quad \text{(B 1)}$$

where C_1 and C_2 are constants, θ is the phase in the periodic depth perturbation (3.22), and $\omega = [gs(n+1/2)k_t]^{1/2}$ and $k_n = k_t/2$ are the resonant edge wave frequency and wavenumber, respectively. Two standing edge wave solutions,

$$\eta_0 = a_0\varphi_n \cos[\omega t - (\alpha_n + |\beta^-_{nn}|)C_{gn}T - \theta_0]\cos(k_n y + \theta/2), \quad \text{(B 2)}$$

$$\eta_0 = a_0\varphi_n \cos[\omega t - (\alpha_n - |\beta^-_{nn}|)C_{gn}T - \theta_0]\sin(k_n y + \theta/2), \quad \text{(B 3)}$$

where a_0 is the amplitude and θ_0 is an arbitrary time phase constant, are found by setting $C_2 = 0$ and $C_1 = 0$ (not at the same time) in (B 1), respectively (the nodes and antinodes in both standing waves occur at the extrema of the perturbed depth (3.22)). The perturbed depth alters the dispersion relation of the standing edge waves with a small frequency shift

$$\begin{aligned}\Omega &= -(\alpha_n \pm |\beta_{nn}^-|)C_{gn} \\ &= -\frac{g}{2C_{gn}}\int_0^{+\infty}\left\{\left[(c_0\varphi_{nx})_x - k_n^2 c_0\varphi_n\right] \pm \left[(c_1\varphi_{nx})_x + k_n^2 c_1\varphi_n\right]\right\}\varphi_n \mathrm{d}x, \end{aligned} \tag{B 4}$$

where + and − signs correspond to (B 2) and (B 3), respectively. The small change in the mean depth c_0 has the same effect on the dispersion relation for both standing edge waves, whereas the periodic perturbation $2c_1\cos(2k_n y + \theta)$ has opposite effects. When $n = 0$, $\varphi_0 = \mathrm{e}^{-k_0 x}$, (B 4) with + sign becomes

$$\Omega = \frac{gk_0^2}{\omega}\int_0^{+\infty} c_{0x}\mathrm{e}^{-2k_0 x}\mathrm{d}x + \frac{gk_0^2}{\omega}\int_0^{+\infty}(c_{1x} - 2k_0 c_1)\,\mathrm{e}^{-2k_0 x}\mathrm{d}x, \tag{B 5}$$

which agrees with the result given by Guza & Bowen (1981) for mode-0 standing edge waves (B 2).

Other interesting solutions are found by setting $C_2 = C_1 = \frac{1}{4}a_0\mathrm{e}^{\mathrm{i}\theta_0}$ and $-C_2 = C_1 = \frac{1}{4}a_0\mathrm{e}^{\mathrm{i}\theta_0}$ in (B 1), resulting in

$$\begin{aligned}\eta_0 = a_0\varphi_n\Big[&\cos(|\beta_{nn}^-|C_{gn}T)\cos(k_n y - \omega t + \alpha_n C_{gn}T + \theta_0) \\ &+ \sin(|\beta_{nn}^-|C_{gn}T)\sin(k_n y + \omega t - \alpha_n C_{gn}T + \theta - \theta_0)\Big],\end{aligned} \tag{B 6}$$

$$\begin{aligned}\eta_0 = a_0\varphi_n\Big[&\cos(|\beta_{nn}^-|C_{gn}T)\cos(k_n y + \omega t - \alpha_n C_{gn}T + \theta - \theta_0) \\ &- \sin(|\beta_{nn}^-|C_{gn}T)\sin(k_n y - \omega t + \alpha_n C_{gn}T + \theta_0)\Big],\end{aligned} \tag{B 7}$$

respectively. Each solution describes two spatially uniform, counter-propagating edge waves with temporally modulated wave amplitudes. The period of the slow energy transfer between the travelling waves is

$$2\pi\left(\epsilon|\beta_{nn}^-|C_{gn}\right)^{-1} = 2\pi\left\{\epsilon\frac{g}{2C_{gn}}\int_0^{+\infty}\left[(c_1\varphi_{nx})_x + k_n^2 c_1\varphi_n\right]\varphi_n \mathrm{d}x\right\}^{-1}. \tag{B 8}$$

Note that energy is conserved (i.e. (2.20) is satisfied). At some times, the oppositely travelling waves have equal amplitude and form a standing edge wave. At other times, the amplitude of one wave vanishes and the wave field is purely progressive. The small change in the mean depth c_0 alters the dispersion relation of both travelling waves but does not affect the wave amplitudes. The undulating bathymetry $2c_1\cos(2k_n y + \theta)$ does not affect the dispersion relation.

With no change in the mean bathymetry ($c_0 = 0$), the above solutions for the spatially homogeneous infinitely long undulating bathymetry correspond to changes in the dispersion relation and temporally constant amplitude ((B 2) and (B 3)) or no changes in the dispersion relation and temporally varying amplitudes ((B 6) and (B 7)). There are no spatially varying solutions. However, standing edge waves with spatially varying amplitudes exist when the perturbed depth (3.22) is periodic in the region $|Y| \geqslant W$ but zero in the region between the undulations $|Y| \leqslant W$. The frequency

detuning Ω must be subcritical but non-zero, and the width W must satisfy

$$W = [(2l+1)\pi - 2\delta]C_{gn}/4\Omega, \quad \delta = \arcsin(K/|\beta_{nn}^{-}|), \tag{B 9}$$

where $K = \alpha_n + \Omega/C_{gn}$, and l is a non-negative integer. When these conditions are satisfied, the standing edge wave solution is

$$\eta_0 = \begin{cases} a_0\varphi_n \mathrm{e}^{-Q(Y-W)} \cos[\omega t + \Omega T + \theta/2 - (l+1)\pi/2] \\ \qquad\qquad \times \cos(k_n y - \delta/2 + \theta/2 - \pi/4), & Y \geqslant W \\ a_0\varphi_n \cos[\omega t + \Omega T + \theta/2 - (l+1)\pi/2] \\ \times \cos\left[k_n y + \Omega/C_{gn}(Y - W) - \delta/2 + \theta/2 - \pi/4\right], & |Y| \leqslant W, \\ a_0\varphi_n \mathrm{e}^{Q(Y+W)} \cos[\omega t + \Omega T + \theta/2 + (l+1)\pi/2] \\ \qquad\qquad \times \cos(k_n y + \delta/2 + \theta/2 + \pi/4), & Y \leqslant -W, \end{cases} \tag{B 10}$$

where $Q = \left[|\beta_{nn}^{-}|^2 - K^2\right]^{1/2}$. The standing wave amplitude is constant over the unperturbed depth section and decays exponentially over the adjacent regions of undulating bathymetry.

REFERENCES

Bowen, A. J. & Inman, D. L. 1971 Edge waves and crescentic bars. *J. Geophys. Res.* **76**, 8662–8671.

Guazzelli, E., Rey, V. & Belzons, M. 1992 Higher-order Bragg reflection of gravity surface waves by periodic beds. *J. Fluid Mech.* **245**, 301–317.

Guza, R. T. & Bowen, A. J. 1981 On the amplitude of beach cusps. *J. Geophys. Res.* **86**, 4125–4132.

Guza, R. T. & Inman, D. L. 1975 Edge waves and beach cusps. *J. Geophys. Res.* **80**, 2997–3012.

Heathershaw, A. D. 1982 Seabed-wave resonance and sandbar growth. *Nature* **296**, 343–345.

Holman, R. A. & Bowen, A. J. 1982 Bars, bumps, and holes: Models for the generation of complex beach topography. *J. Geophys. Res.* **87**, 457–468.

Huntley, D. A., Guza, R. T. & Thornton, E. B. 1981 Field observations of surf beat 1. Progressive edge waves. *J. Geophys. Res.* **86**, 6451–6466.

Lippmann, T. C. & Holman, R. A. 1990 The spatial and temporal variability of sand bar morphology. *J. Geophys. Res.* **95**, 11575–11590.

Liu, P. L.-F. & Cho, Y.-S. 1993 Bragg reflection of infragravity waves by sandbars. *J. Geophys. Res.* **98**, 22733–22741.

Mei, C. C. 1985 Resonant reflection of surface water waves by periodic sandbars. *J. Fluid Mech.* **152**, 315–335.

Mei, C. C. & Liu, P. L.-F. 1993 Surface waves and coastal dynamics. *Ann. Rev. Fluid Mech.* **25**, 215–240.

Munk, W., Snodgrass, F. & Gilbert, F. 1964 Longs waves on continental shelf: An experiment to separate trapped and leaky modes. *J. Fluid Mech.* **20**, 529–553.

Oltman-Shay, J. & Guza, R. T. 1987 Infragravity edge wave observations on two California Beaches. *J. Phys. Oceanogr.* **17**, 644–663.

Rey, V., Guazzelli, E. & Mei, C. C. 1996 Resonant reflection of surface gravity waves by one-dimensional doubly sinusoidal beds. *Phys. Fluids* **8**, 1525–1530.